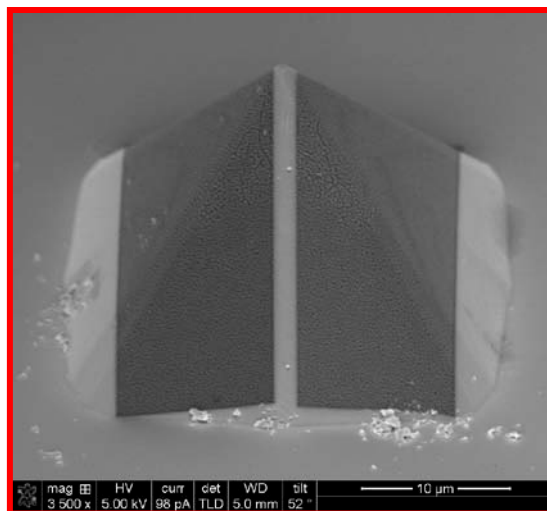


2010

NANO ELECTRONICS.

# Controlling the magnetization at the conical apex of a multi-terminal STM probe

Michel Zoontjes



Graduation Commission:  
Prof. dr. ir. W.G. Van der Wiel  
Prof. dr. ir. P.J. Kelly  
Dr. ir. I. Vera Marún  
Ing. M.H. Siekman  
Ing. J.G.M. Sanderink



# Controlling the magnetization at the conical apex of a multi-terminal STM probe

Master thesis of M.G.C. Zoontjes

2010

## Supervisors:

Prof. dr. ir. W.G. Van der Wiel  
Dr. ir. I. Vera Marun

## Graduation Commission:

Prof. dr. ir. W.G. van der Wiel  
Prof. dr. ir. P. Kelly  
Dr. ir. I. Vera Marun  
Ing. M.H. Siekman  
Ing. J.G.M. Sanderink

This thesis is a result of the work I did in the NanoElectronics group for my master Nanotechnology at the University of Twente. The research was based on the promotional research of I. Vera Marun.

NANO ELECTRONICS.

**MESA+**

---

Institute for Nanotechnology



### ABSTRACT

The goal of the thesis was to control this magnetization at the conical apex of the SF-STM tips. Spin-Filter Scanning tunnel microscopy is a new principle to characterize the magnetization of a sample. First measurements show an out-of-plane magnetization at the conical apex of the tips, where we would like to have an in-plane magnetization.

Small tips of silicon were made to mimic the SF-STM tips. These tips have a similar apex as the double tips. At these tips a metal layer stack contains 10 nm gold, 2 to 10 nm cobalt and 5 nm gold were evaporated. First measurements at these tips by magnetic force microscopy confirmed the out-of-plane magnetization at the conical apex of the tips. To be able to control the magnetization anisotropy has been introduced to get an in-plane easy-axis for the magnetization at the conical apex. This is done by introducing evaporation anisotropy and shape anisotropy. Both methods have been characterized separately, before they were combined at one tip.

Evaporation anisotropy was introduced in the cobalt layer by applying a magnetic field during evaporation of the metal layer stack. VSM measurements showed a uni-axial anisotropy parallel to the applied field. By introducing the evaporation anisotropy at a tip, the remanence of the magnetization was increased.

Shape anisotropy was introduced by using the focused ion beam (FIB). First the shape anisotropy has been applied at different sizes strips, to test the effect of the shape in combination with the length/width ratio. These measurements show a strong anisotropy in the strips. By introducing it to the tips, there was an increase of magnetic remanence visible, but this was not strong enough for an in-plane magnetization at the conical apex.

As last step, both anisotropies have been combined at a tip. A strip was made parallel to easy-axis of the evaporation anisotropy. A strong in-plane magnetization was visible and a strong field was needed to switch the magnetization.



## CONTENTS

<b>Abstract</b> .....	<b>5</b>
<b>Contents</b> .....	<b>7</b>
<b>1. Introduction</b> .....	<b>9</b>
1.1 Scanning tunneling microscopy (STM) .....	9
1.2 Spintronics.....	10
1.3 Spintronics in STM techniques .....	11
1.4 Spin-filter scanning tunneling microscopy. ....	12
1.5 Controlling the magnetization at the tip. ....	14
<b>2. Nanomagnetism</b> .....	<b>15</b>
2.1 Magnetic domains .....	15
2.2 Origin of magnetic domains .....	16
<b>3 Materials and Methods</b> .....	<b>18</b>
3.1 The tip.....	18
3.2 Fabrication process for the small tip .....	19
3.3 Characterization of the tip magnetization .....	21
3.3.1 Atomic Force Microscopy .....	21
3.3.2 Magnetic Force Microscopy .....	22
3.3.4 The measurements setup.....	23
3.3.5 Vibrating Sample Magnetometer .....	24
<b>4. Results and Discussion</b> .....	<b>25</b>
4.1 Tip fabrication .....	25
4.1.1 Defining the shape of the conical apex .....	25
4.1.2 Evaporation vs. Sputtering .....	27
4.2 Characterization of the magnetization in the conical apex.....	29
4.2.1 Measurements at the double tip pyramid .....	29
4.2.2 Measurement at a small pyramid. ....	29
4.3 Influencing the magnetization direction at the conical apex of the pyramid. ....	31

4.3.1	Evaporation anisotropy .....	31
4.3.2	Evaporation anisotropy at the magnetic pyramid. ....	35
4.3.3	Shape anisotropy .....	36
4.3.4	Shape anisotropy at the pyramid .....	38
4.4	Combine shape anisotropy and evaporation anisotropy .....	43
<b>5</b>	<b>Conclusion &amp; Recommendations .....</b>	<b>45</b>
5.1	Conclusion .....	45
5.2	Outlook .....	46
<b>6</b>	<b>Literature.....</b>	<b>48</b>
	<b>Acknowledgements.....</b>	<b>49</b>
	<b>Appendix A: Mask .....</b>	<b>50</b>
	<b>Appendix B: Cleanroom Process.....</b>	<b>51</b>

## 1. INTRODUCTION

In the development of hard disk recording, recording densities are increasing continually. To be able to characterize high-density data, new techniques are needed which have a high resolution to measure the magnetization. In data storage it is required to be able to characterize next to the feature size, also the magnetic information of the data. Spin-filter scanning tunnel microscopy is a new technique, which is able to characterize magnetization with high resolution over an area [1].

### 1.1 SCANNING TUNNELING MICROSCOPY (STM)

Scanning tunneling microscopy (STM) is a powerful tool to characterize substrates at atomic resolution. The basics for STM lay in quantum mechanics, which shows that electrons are able to propagate between two contacts if they are separated by a thin insulator. In the classical situation the energy of the electrons is not high enough to overcome the energy barrier created by the insulator [2]. In the quantum mechanics because the wave property of electrons results in that the electrons are able to tunnel through the barrier. This is shown in Fig. 1.



Figure 1: Schematic overview of the difference for the classical and quantum mechanical image of impenetrable barrier. In the classical situation there is no possibility to pass the wall, but by quantum mechanics it is possible to tunnel [2].

In 1981 the first STM was developed by Gerd Binnig and Heinrich Rohrer, for which they received the Nobel Prize for physics in 1986 [2]. In an STM, a sharp tip is scanning the surface at a small distance of the surface, see Fig 2. By applying a voltage between the tip and the surface, electrons tunnel from the surface to the tip. In the constant-current mode, the STM keeps the tip at a constant height of the surface. If the surface has a step, the tunneling current will increase, because the insulating barrier is thinner. Then the feedback loop will lift the tip, so that the tunneling current is at the set point again. The feedback signal represents the topography of the surface.

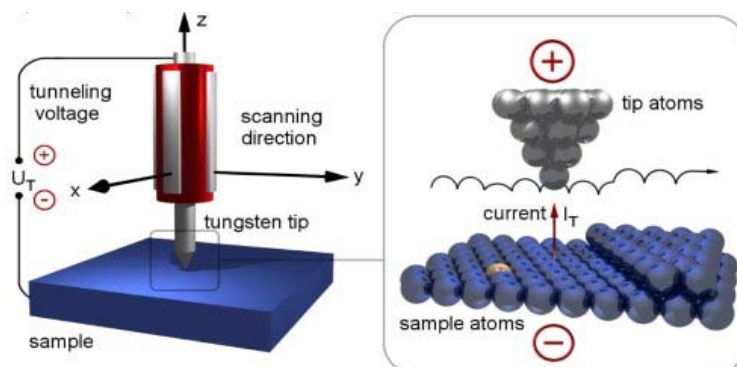


Figure 2: Schematic overview of an STM [3]

## 1.2 SPINTRONICS

In the late 1980's a new area of electronics arose: spintronics. In conventional electronics, the charge of electrons is used as carrier, whereas in spintronics also the electron spin is being applied. Giant magnetoresistance (GMR) is a well known spintronics effect, and is applied in read heads of hard disks nowadays [17]. In a GMR junction two ferromagnetic contacts are separated by a non-magnetic metal layer. If a current is propagating through the junction there is a difference in the resistance for a parallel and anti-parallel configuration of the magnetization of the ferromagnetic contacts.

Next to GMR there is also tunnel magnetic resistance (TMR), where the non-magnetic layer between the two ferromagnets is an insulating layer. Here, there is no electron conduction between the ferromagnetic contacts, but they tunnel through the thin insulator barrier. The ferromagnetic contacts can have two different magnetization configurations, viz. a parallel and an anti-parallel configuration. The two configurations have a difference in resistance and this can be used to distinguish between the parallel and anti-parallel configuration. The differences in resistance can be expressed by Equation (1) [4].

$$TMR = \frac{\Delta R}{R_{\uparrow\uparrow}} = \frac{R_{\uparrow\downarrow} - R_{\uparrow\uparrow}}{R_{\uparrow\uparrow}} \quad (1)$$

The resistance change between the two configurations can be explained by the density of states (DOS) diagrams, which are shown in Fig. 3. Here both configurations are shown, with their corresponding DOS diagrams. A basic property of a ferromagnet is that they have a different number of spin-up and spin-down electrons, which result in magnetization in the direction of the largest number of spins. If the contacts are magnetized anti-parallel, at contact 1 there are more spin-up electrons than spin-down electrons available for tunneling, but at contact 2 there are more vacancies for spin-down than for spin-up electrons available to tunnel to. This means that the total amount of electrons which can tunnel is small, and this results in a higher resistance. If the contacts are parallel magnetized then there are at contact 2 enough vacancies with the right spin, for the majority spin-electrons which are at the first contacts. This results in a smaller resistance, and the difference in resistance between the parallel and anti-parallel configurations leads to a TMR.

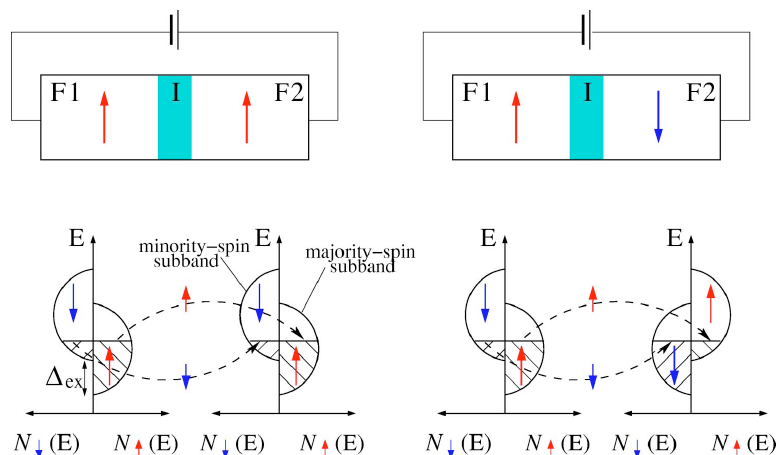


Figure 3: Two configurations of the magnets in a Magnetic Tunnel Junction (MTJ) with the corresponding DOS diagrams [4].

### 1.3 SPINTRONICS IN STM TECHNIQUES

Spintronics is applied in scanning tunnel microscopy to be able to characterize the magnetization of a nanoscale sample. The spin-polarized STM (SP-STM) uses the working principle of a conventional STM, but combined with a magnetic tip it is possible to measure the magnetization of a sample [5]. The SP-STM is shown in Fig. 4. The working principle of the SP-STM can be compared to a magnetic tunnel junction, where the magnetic surface and the magnetic tip are each one of the two ferromagnetic contacts and the vacuum gap between the tip and the surface is the insulating layer. So, if the magnetization of the tip is parallel to the magnetization of the surface, the tunnel current is higher than if the surface and tip magnetizations are in an anti-parallel configuration. Here one difficulty occurs, namely the topography of the surface. If there are steps in the surface the tunnel current will be influenced by the distance change between substrate and tip on one hand, and the magnetization of the substrate on the other hand. As there could be two different contributions to the variation in tunnel current, it is hard to scan the magnetic domains at large scale [5].

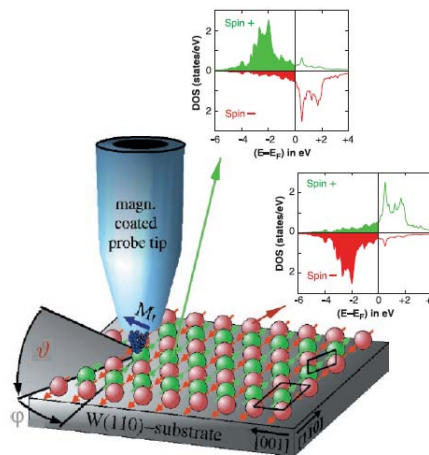


Figure 4: Working principle of a spin-polarized STM. [6]

Another technique that can analyze magnetization at an atomic scale is ballistic electron magnetic microscopy (BEMM), which is based on the principle of ballistic electron energy microscopy (BEEM) [7]. BEEM is developed to study the interface of a metal-semiconductor interface. Here (hot) electrons tunnel from the STM tip into the metal and propagate further to the semiconductor. The electrons in the metal need certain energy to overcome the Schottky barrier at the metal-semiconductor interface. An overview of the setup and the band diagram is shown in Fig. 5.

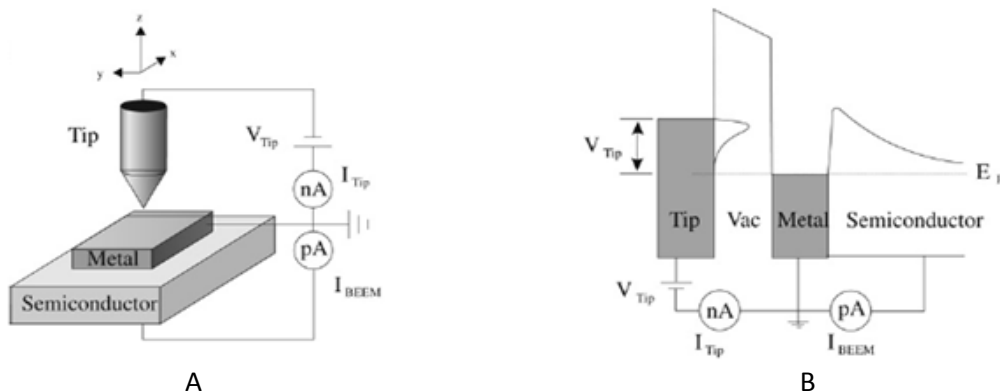


Figure 5: a) Setup of a BEEM measurement [7]. b) Band diagram of a BEEM barrier with a Schottky barrier at the metal-semiconductor interface [7].

In the case of BEMM, at the doped semiconductor substrate a metal layer stack with two ferromagnetic layers and three non-magnetic layers are evaporated [8]. This is shown in Fig. 6. The ferromagnetic layer closest to the semiconductor has the function of an analyzer; the non-magnetic layers are spacers, and the top ferromagnetic layer top as a polarizer. The polarizer layer is the ferromagnetic layer which has to be characterized. Between the STM tip and the ferromagnetic layer a tunnel current is send and the measured current depends on the configuration of the two ferromagnetic layers. If the magnetization of the analyzer is known, the magnetization of the polarizer can be determined. If the top ferromagnetic layer has a parallel magnetization, the measured current is high. If the polarizer has an anti-parallel configuration the electrons are scattered between the ferromagnets and a low current is measured.

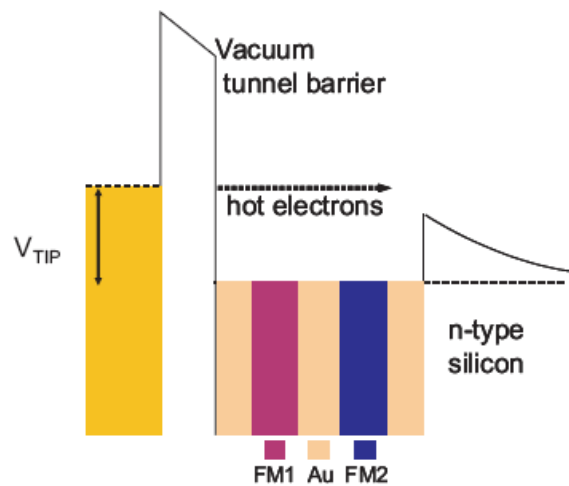


Figure 6: principal of BEMM, where the polarizer and analyzer are ferromagnetic layers and the spacer is a non-magnetic metal.

#### 1.4 SPIN-FILTER SCANNING TUNNELING MICROSCOPY.

Like the SP-STM the spin-filter STM (SF-STM), the technique applies spin-polarized tunneling between the tip and the substrate. The novelty lies in the electron spin analyzer. In the SF-STM the electrons tunnel from the substrate to the tip and then in the tip the electron spin is analyzed. Two currents are measured: the tunnel current  $I_T$  and the collector current  $I_c$ . An advantage of measuring the two currents separately is that the  $I_T$  is used for the topography and the  $I_c$  is used to analyze the spin of the electrons. By have a separate current for the topography it is possible to measure the magnetization over a large area.

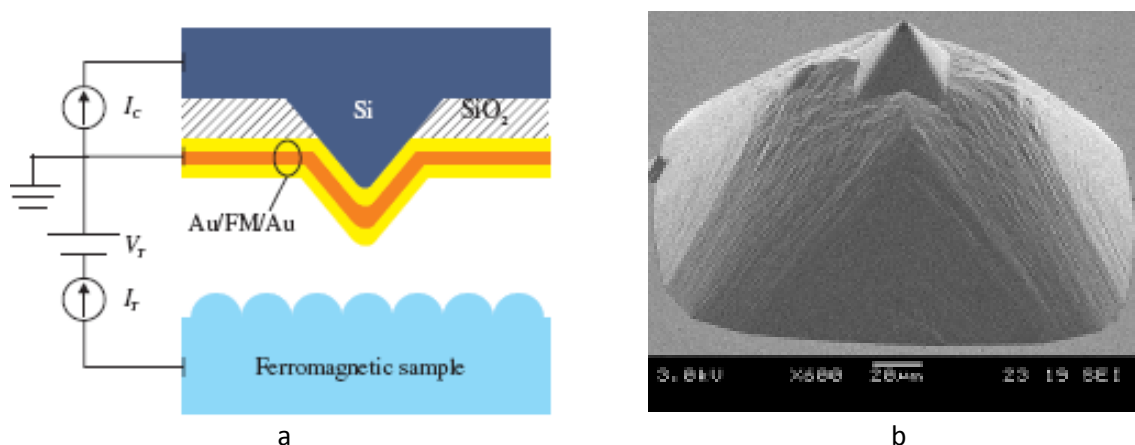


Figure 7: a) Schematic overview of the SF-STM principle [9]. b) SEM image of the double tip [9].

For the spin-analysis the principle of hot electrons from the BEMM is used, to distinguish spin-up and spin-down electrons. Electrons are tunneling from the substrate to tip. The measured tunnel current  $I_T$  does not depend at the magnetization of the substrate and it gives the topological information of the substrate. The tunneled electrons, which are (partly) spin polarized in case of a ferromagnetic substrate, are now propagating in the metal layer stack to the semiconductor. Here the spin-analysis is done. During the propagation of the electrons in the ferromagnetic layer in the tip attenuation will occur due to scattering.

The transmission probability of electrons decays exponentially with the attenuation length  $\lambda$ . In ferromagnetic layers this length for majority spin electrons is longer than the length for the minority electrons. Therefore, electrons with a spin which is anti-parallel to the ferromagnetic layer in the tip will scatter more and lose more energy than the spin-up electrons, and they are not able to overcome the Schottky barrier [16]. The electrons with a spin parallel to the ferromagnetic layer keep enough energy to overcome the barrier and are collected by the semiconductor. There the electrons are collected in the  $I_C$ .

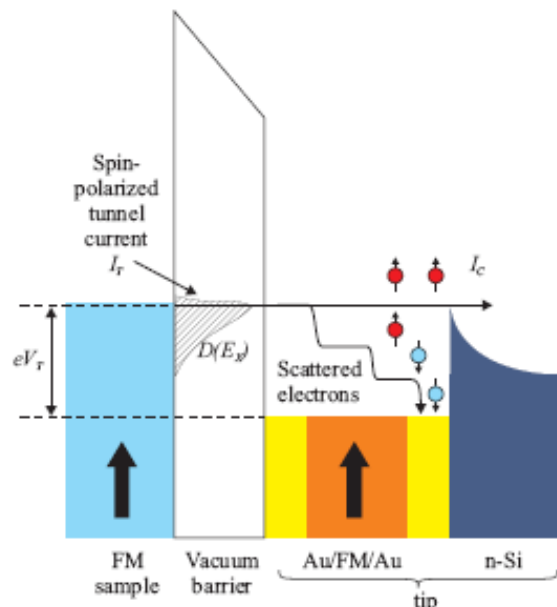


Figure 8: Energy diagram in a SF-STM measurement. Electrons with an anti-parallel spin scatter in the ferromagnetic layer of a SF-STM, while the electrons with a parallel spin have enough energy to overcome the Schottky barrier [9].

First SF-STM measurements performed by Iván Vera Marún showed that the principle of the SF-STM works, see Fig. 9. Measurements done at a perpendicular magnetized Co/Pt multilayers were compared with magnetic force measurements. The measurements showed that the pattern of the magnetization by SF-STM, can be compared with the pattern measured by the magnetic force microscopy.

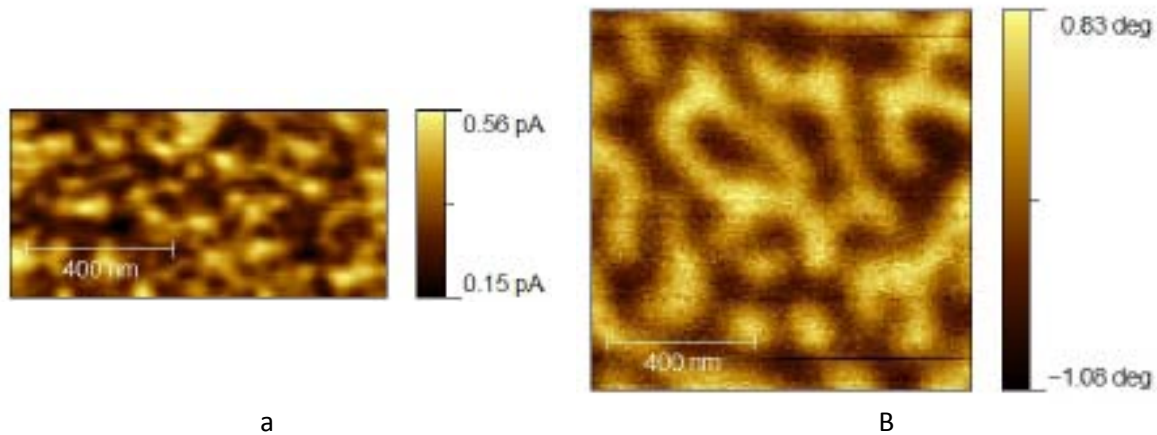


Figure 9: a) Preliminary measurements performed at a Co/Pt multilayer done by SF-STM [9]. b) Measurements at the same sample by magnetic force microscopy [9].

### 1.5 CONTROLLING THE MAGNETIZATION AT THE TIP.

A part that is not solved is to control the magnetization direction in the conical apex of the small tip. First characterization of the magnetization by Iván shows an out-of-plane magnetization. With these tips it is only possible to measure magnetic domains that are out-of-plane magnetized, whereas we also like to characterize samples with an in-plane magnetization. Therefore a modification of the ferromagnetic layer at the apex of the tip is needed, so that an in-plane easy-axis is introduced. Then the magnetization will probably prefer to lie along the easy-axis in the cobalt layer.

The place of the tip that is used as spin-filter is the conical apex of the small tip. The plan is to mimic the SF-STM tip, by making the tips, which are similar to the small tip at the double tips. These small tips can be used as platform for the metal layer stack. This metal layer stack is similar as the metallic layer stack used in the SF-STM, namely first a layer of 10 nm gold, then a cobalt layer with a thickness between the 2 nm and 10 nm and at last a 5 nm gold capping layer.

The first part is to characterize the magnetization of the cobalt layer at the tips. When the magnetic characteristics mimic the results of the double tips, the start can be made to control the magnetization direction of the tips.

To introduce an easy-axis in the cobalt layer, the goal is to use evaporation anisotropy and shape anisotropy. The evaporation anisotropy could be done by a magnetic field during the deposition. The metal layer stack will be shaped by the use of a focused ion beam. The effects of both anisotropies are characterized separately, before combining them both at one tip. Characterization is done by magnetic force microscopy.

## 2. NANOMAGNETISM

### 2.1 MAGNETIC DOMAINS

To control the magnetization orientation in the tip, some knowledge of basic magnetism is needed. An important property of magnetic materials is that at small scale domains are formed to reduce the total energy of a system. Another important property of the magnetization direction is magnetic anisotropy, which can have different origins, such as crystal anisotropy and shape anisotropy. Strong anisotropy results in an easy-axis of a ferromagnetic layer, which is the preferable direction of the magnetization. If there is weak anisotropy, there is no specific easy-axis and then the domains are formed to reduce the stray field. In Fig. 10 the situation for weak and strong anisotropy in a rectangular and circular film are shown. In the case of weak anisotropy, which is the case in Figs. 10a and 10b, there is no easy-axis in the film. So the magnetization has no preferable direction. In this case it is energetically more favorable to form magnetic domains, than to have a stray field outside the ferromagnet. In the case of strong anisotropy, the magnetization lies in the direction of the easy-axis. This can be seen in Figs. 10c and 10d. In these cases it costs less energy to have a stray field outside the ferromagnetic film, than to form extra domain walls.

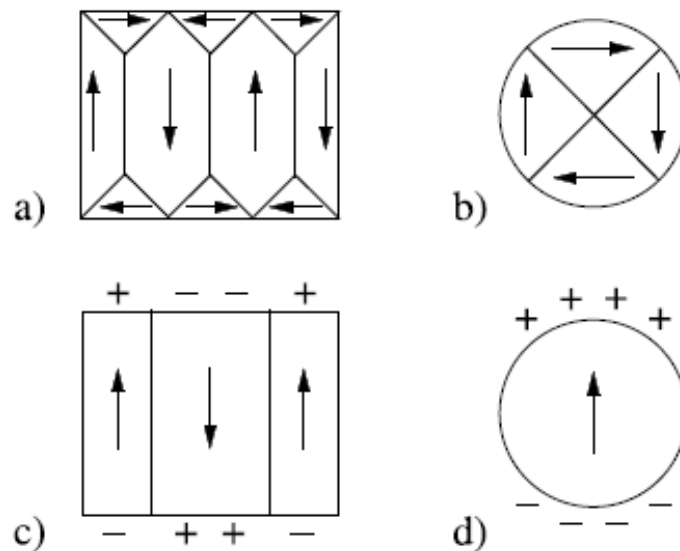


Figure 10: Situation of a rectangular and circular ferromagnetic film in the cases of a weak and strong anisotropy. In a) and b) there is a low anisotropy and domains are formed to reduce the stray field energy. In c and d there is a strong anisotropy and the magnetization prefers to orient along the easy-axis with a stray field [10].

The domains are separated by domain walls. In Fig. 11 an example of a domain wall, a so-called Bloch wall is shown. Here at each of the edges of the wall there is a magnetization in the direction of the easy axis. These magnetizations have an angle of  $180^\circ$ . The domain wall is not an abrupt border between the two magnetizations, but the magnetization is turning over multiple atoms. The thickness of the wall depends on the energy it costs to make the wall. Domain wall costs energy due to the rotation of the magnetization over the wall and this increases the exchange energy in the system.

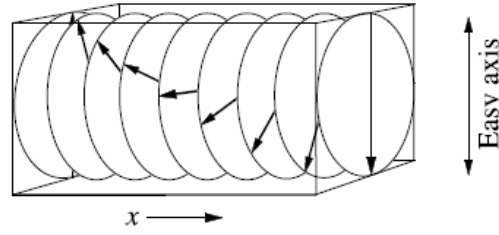


Figure 11: An example of a domain wall is the Bloch wall [10].

## 2.2 ORIGIN OF MAGNETIC DOMAINS

The total energy balance of a magnetic system is depending on more factors than the crystal anisotropy and the stray field. There are in total six different contributions to the total free energy of a ferromagnetic system. The equation for the total free energy of a system is an integral of the sum of these different contributions [10]:

$$E_{\text{tot}} = \int \left[ \underbrace{A(\text{grad } m)^2}_{\text{exchange}} + \underbrace{F_{\text{an}}(m)}_{\text{anisotropy}} - \underbrace{H_{\text{ex}} \cdot J}_{\text{ext. field}} + \underbrace{\frac{1}{2} H_d \cdot J}_{\text{stray field}} - \underbrace{\sigma_{\text{ex}} \cdot \epsilon^0}_{\text{ext. stress}} + \underbrace{\frac{1}{2} (p_e - \epsilon^0) \cdot c \cdot (p_e - \epsilon^0)}_{\text{magnetostrictive}} \right] dV \quad (2)$$

Here the exchange energy favor aligned spins in a ferromagnet, and  $A$  here is a material constant.  $F_{\text{an}}$  in the anisotropy term collects the contributions from crystal and structural magnetic anisotropies, but shape anisotropy is not included in this term. The external field is also called the Zeeman energy and it collects the contribution of an applied field at the magnetic domains. The most important term which can be influenced is the stray field term, because in this term the shape anisotropy and the energy which contribute from the stray field are included. The external stress term collects all stress of non-magnetic origin.  $\epsilon^0$  is the free magneto-elastic deformation at any given point and in the magnetostrictive term  $c$  is the tensor of elastic constants.  $p_e$  is asymmetric tensor, which is the actual distortion. There is not a separate energy term for the forming of the domain walls, but domain wall energy can be included in the exchange term and the anisotropy term.

An example of different magnetic domain structures is simulated for a strong uni-axial cubical system. The easy-axis is oriented parallel to one of the edges of the cube. Here a phase diagram is presented for two variables, viz. the particle size and the magnetic anisotropy  $Q$  of the particles. The size is a function of the exchange energy  $A$  and the stray field energy. If a larger size particle there is more space to rotate the magnetization over more atoms. The magnetic anisotropy  $Q$  is defined as  $Q = K_u/K_d$ , where  $K_u$  is the crystal anisotropy and the  $K_d$  the stray field term. In the phase diagram different phases appear. If the particle size is small, a single domain (SD) will form. If the  $Q$  is high the magnetization will lay parallel to easy-axis of the cubical system. If the size increases, multiple domains will form. Here, it will be energetically more favorable to reduce the stray field and form domain walls in the structure. In the case of a high  $Q$  and increasing size, the single domain will develop to a two domain and further increase results in a multiple domain structure. Here, the stray field will be larger than in the multiple domain wall phases when there is a low magnetic anisotropy. In that case also domain walls will form, but the stray field is minimized. Also there is a possibility for a vortex state (V). This occurs when there is no preferable anisotropy available, and there is no easy-axis. Here the magnetization is circling around the center of the cubical particle.

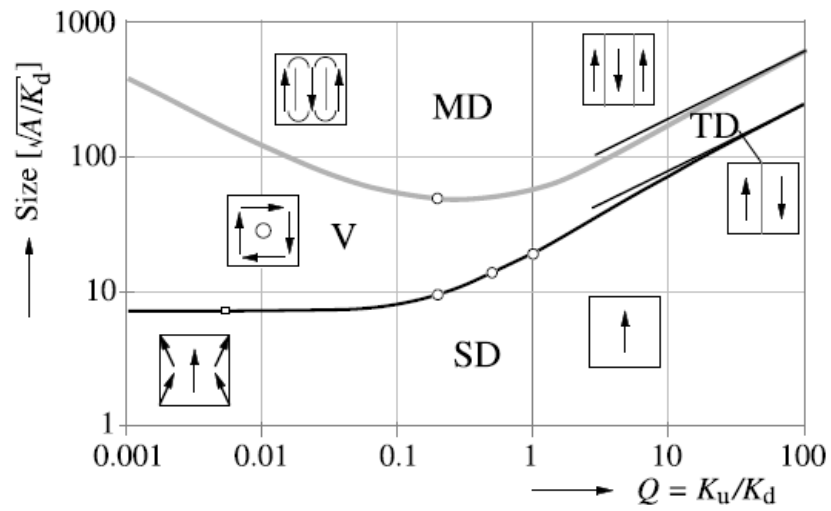


Figure 12: Phase diagram of a simulated uni-axial anisotropic cubical particle. The presence of a single domain phase (SD), two domains phase (TD), multiple domains phase (MD) or a vortex state (V) depends at the relation between the size and the magnetic anisotropy [10].

### 3 MATERIALS AND METHODS

#### 3.1 THE TIP

The tip of the SF-STM has a double tip design, see Fig. 13. The goal of the assignment is to control the magnetization at the conical apex of the small pyramid, so that it will be an in-plane magnetization oriented along the easy-axis. For that small tips are fabricated to investigate the requirements. Therefore, only the part of the process for the small tip is used and for this Iván's mask for the small pyramids is used. The complete mask lay-out is given in appendix A, but in Fig. 14 a close-up of the pattern is shown. For the small tips a circle with a 10  $\mu\text{m}$  diameter is required.

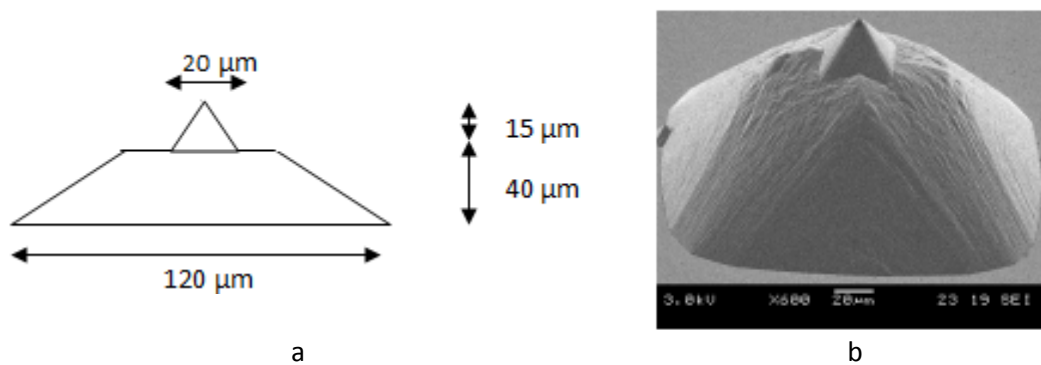


Figure 13: a) Overview of the double tip used in the SF-STM. b) SEM image of the double tip.

The mask for the small tip mainly consisted of 10  $\mu\text{m}$  circles in sets of three, see Fig. 14a. The mask also contains circles with a diameter of 15  $\mu\text{m}$  and 40  $\mu\text{m}$ , but these are not used in this assignment. The 15  $\mu\text{m}$  circles can be used as back up in the KOH etching process. If the etching of the silicon is not stopped before the caps are removed, there is a possibility to use the 15  $\mu\text{m}$  circles to make the pyramids. The pyramids will be a little bit higher, but the conical apex itself should not be different, in comparison with the conical apices formed with the 10  $\mu\text{m}$  pattern.

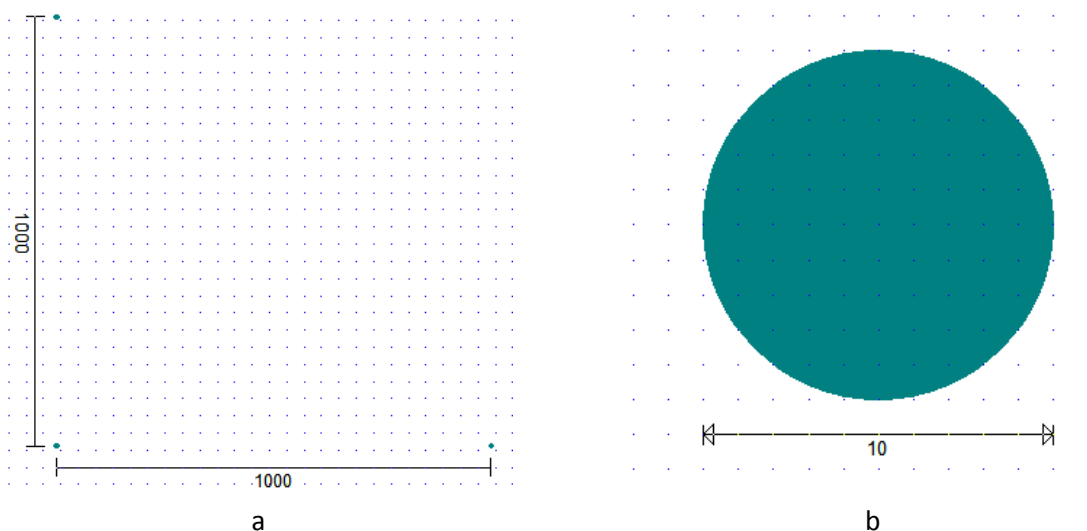


Figure 14: The 10  $\mu\text{m}$  circles pattern of the used mask for the lithography step. a) The distribution of the circles. b) 10  $\mu\text{m}$  circle.

### 3.2 FABRICATION PROCESS FOR THE SMALL TIP

The process for the small tips consists of a one-step lithography process. The fabrication process needs several steps. A detailed recipe is included in Appendix B, but the main steps are explained here.

As substrate a 100-silicon wafer is chosen. First by a local oxidation of silicon (LOCOS) step a 50 nm thick silicon oxide layer is grown, and on top of this a 160 nm silicon nitride layer is deposited. The LOCOS step is a dry oxidation step of the silicon.

Then a photoresist layer is spun at the wafer and by UV light exposure the pattern of the photomask can be transferred into the photoresist. After resist development the pattern in the photoresist can be transferred into the silicon oxide and silicon nitride by dry etching. The goal is that the overetching of this step is not too high, but one has to be sure that at least the silicon nitride is etched away. This has to do with the next step, where the silicon is etched with KOH.

The next step is to etch the silicon to the pyramid shape. This is done by wet etching in KOH, which is an isotropic etch alongside the 111-planes of the silicon crystal. This results in a pyramid shape of the silicon. The etching is not only along the Si 111-planes, but also slow horizontal etching occurs under the nitride cap. This is important to make the conical apex of the pyramid smaller. The rate of underetching of the silicon will be about 0.5  $\mu\text{m}/\text{min}$ . The goal is to keep a 1  $\mu\text{m}$  connection between the silicon and the silicon oxide. It is required that the nitride cap keeps attached to the pyramid.

The following step is oxidation of the silicon by a LOCOS step. This is important to shape the conical apex of the pyramid round. To do this a 300 nm thick silicon oxide layer needs to be grown. During the oxidation of the silicon, there will oxygen diffusion under the nitride cap and this is responsible for rounding of the tip. This step is shown in Fig. 15 in more detail. Due to the diffusion of oxygen under the nitride two 'bird beaks' are formed at the sides of the pyramid. These bird beaks are important for the round shape at the end of the process. The goal is to let the bird beaks touch with the LOCOS step, so that the shape of the tip is rounded. If the LOCOS step is too long and the beaks overlap, the tip will get a sharp end. If the beaks do not touch the middle of the tip will stay flat. The end result of the LOCOS step is strongly depended of the etching step with the KOH.

The next step is to remove the silicon nitride cap and the oxide layer. The nitride cap can be removed by  $\text{H}_3\text{PO}_4$ . If the nitride cap is removed, what remains is a silicon tip, with a silicon oxide cap. The next step is to remove the silicon oxide layer, to bare the silicon tip. For the SF-STM tip is needed that the metal stack is in direct contact with the conical apex of the silicon pyramid. How much silicon has to be made free of the silicon, will influence the etch time in the BHF. In this assignment no isolation is needed, because the goal is to characterize the magnetization of the cobalt layer, and no electrical experiments are done with these tips. For that the complete layer of oxide can be etched away. If the electrical properties are important, there is a possibility to leave a piece of the oxide layer as isolation layer between the metal layer stack and the silicon. The oxide layer at the top of the pyramid is thinner than the oxide layer at the sides of the pyramid, so by the etch time the connection surface can be determined.

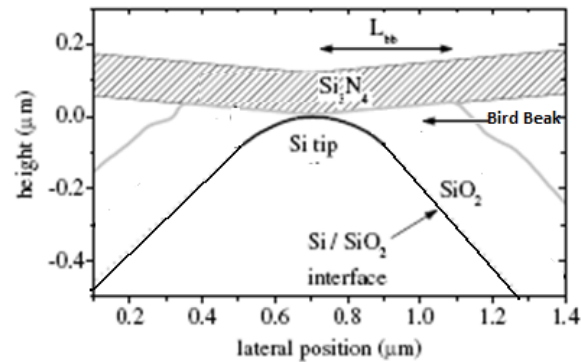


Figure 15: Rounding of the STM by the LOCOS step in the process [9].

The next step is to deposit a metal layer stack at the silicon pyramid. This could be done by e-beam evaporation by the DCA and or thermal evaporation by Sputterke. A large difference between the methods is the deposition direction. Sputtering has a higher deposition rate and no directionally, which will prevent anisotropy by depositing. Evaporation is done under an angle, which can cause anisotropy due the depositing. The anisotropy occurs due a small difference in thickness of the metals at the pyramids. This can be prevented by rotating the sample holder during the evaporation. Also is it possible to apply a magnetic field, which can give anisotropy in the magnetic layer. This is done due the sample holder contain magnets.

1.		<ul style="list-style-type: none"> <li>• Use LOCOS to form a 50 nm silicon oxide layer</li> <li>• Deposit a 150 nm silicon nitride layer</li> </ul>
2.		<ul style="list-style-type: none"> <li>• Transfer the pattern of the mask with a photolithography step.</li> <li>• Use RIE to etch the silicon nitride layer</li> <li>• Remove the oxide</li> </ul>
3.		<ul style="list-style-type: none"> <li>• Etch step to etch the silicon with KOH</li> </ul>
4.		<ul style="list-style-type: none"> <li>• Use a LOCOS step to form a 300 nm silicon oxide layer</li> </ul>
5.		<ul style="list-style-type: none"> <li>• Remove the nitride cap with H3PO4</li> <li>• Remove the oxide layer with BHF</li> </ul>
6.		<ul style="list-style-type: none"> <li>• Evaporation of the metal layer stack:                             <ul style="list-style-type: none"> <li>○ 10 nm gold</li> <li>○ 2-10 nm cobalt</li> <li>○ 5 nm gold</li> </ul> </li> </ul>

The metal layer stack consists of three layers. The first layer is a 10 nm gold layer. This layer is a separation layer between the cobalt and silicon to prevent the formation of cobalt silicate. The second layer is the ferromagnetic cobalt layer. The goal is to use a Co layer with a thickness of around 2 to 10 nm. The cobalt layer is capped with a 5 nm gold layer.

### 3.3 CHARACTERIZATION OF THE TIP MAGNETIZATION

For analyzing magnetic domains a number of techniques are available, a short overview is shown in Fig. 16. Most techniques are lacking resolution for analyzing the magnetic structures. Because the conical apex of the tip is smaller than 1  $\mu\text{m}$ , a resolution of tens of nanometers is preferable to characterize the magnetic properties of the tip. Magnetic force Microscopy is a high resolution technique and it is easy to use [11].

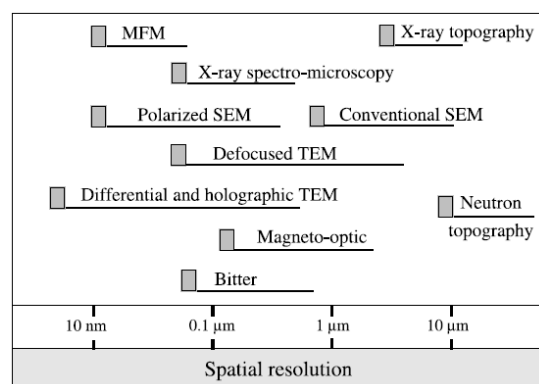


Figure 16: Overview of different techniques to measure the magnetization. MFM is a measurement technique with a high resolution [11].

#### 3.3.1 ATOMIC FORCE MICROSCOPY

The AFM consists out of a cantilever with at the end a sharp tip. This tip is probing the surface and the deflection of the tip is measured by a laser, which is reflecting in a photodiode, see Fig. 17.

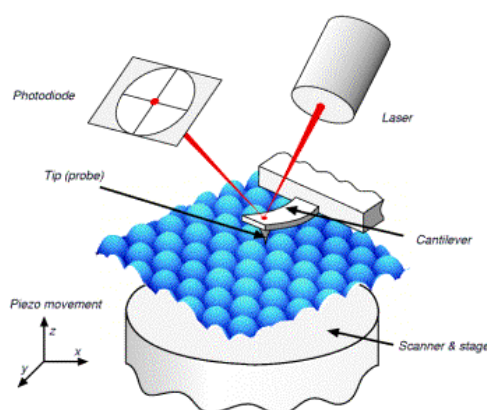


Figure 17: Schematic overview of an AFM [12].

The two most used modes of the AFM are contact mode and tapping mode. In contact mode the tip is scanning over the surface, and if there is a step in the surface the cantilever is deflecting and a feedback system is correcting the height of the cantilever. This feedback signal represents the step height in the surface. In tapping mode the cantilever is brought into resonance and when there is a

height difference the tapping amplitude change. The feedback signal is the correction of the amplitude by changing the height of the cantilever, so the amplitude is back at its set point.

### 3.3.2 MAGNETIC FORCE MICROSCOPY

Magnetic force microscopy (MFM) is a modification of the AFM, where a magnetic tip is used as probe [13]. MFM can measure the magnetic stray fields of a magnetic sample, which can be done, like the AFM, in static or in dynamic mode. For a higher sensitivity mainly the dynamic mode is used.

The magnetic forces applied by the stray fields to the tip, are much weaker than other forces, like Vander Waals forces, capillary forces and adhesion forces. Close to the surface the magnetic forces are hard to measure. Therefore a two trace measurement is used for imaging the magnetic forces. During the first trace, a normal AFM image is made of the surface. By the second trace the tip is lift off a certain distance of the surface and with the topography of the surface in its memory it measure the change in amplitude depends only at the stray fields of the magnetic sample.

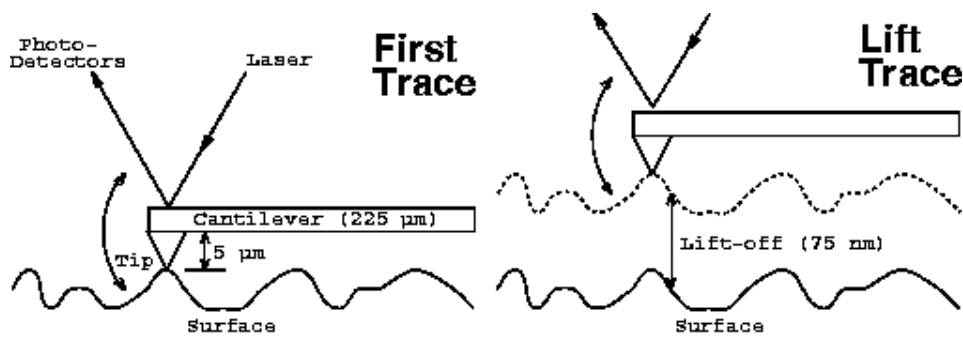


Figure 18: scanning by the MFM mode. First a topographic scan is made, and then this is used for the lift trace.

The magnetic tip is sensitive to the changes in the z-component of the force applied the stray fields. The change of the magnetic stray fields can be measured if it is in plane with the magnetization of the tip, which is often vertically magnetized. Changes in the stray field, resulting in a changing spring constant of the cantilever, expressed by the following formula:

$$c_F = c - \frac{\partial F}{\partial z} , \quad (3)$$

where  $c$  is the natural spring constant of the tip and  $dF/dz$  the derivative in the same direction of the magnetization of the tip. If the spring constant becomes larger, in dynamic mode the amplitude of the tip will decline. If the spring constant becomes smaller, the cantilever is softer and the amplitude of the movement is larger.

The stray field with its separate components in x- and z-direction is shown in Fig. 19. The magnetic forces applied by the stray field, are much weaker than the other forces as the Van der Waals forces, capillary forces and adhesion force. Close to the surface the magnetic forces are too weak for sensing the tip, but because of the stray field there is a long range coupling between sample and probe, and it is possible to measure the magnetic force a distance above the surface.

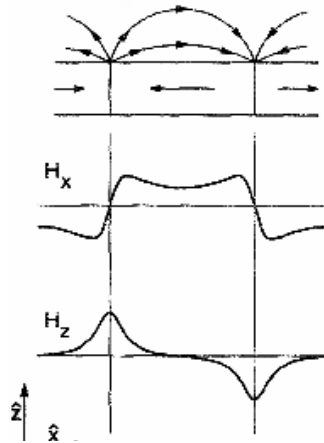


Figure 19: Domain walls with the stray field and the  $x$  and  $z$  components of the stray field. The MFM is only sensible for the  $z$ -component of the stray field [13].

The tip will be attracted to the surface if the stray field has the same direction as the magnetization of the tip. If the sample is in-plane magnetized, above the domain the stray field is not parallel to the tip. However, at the domain walls the stray field is vertical, and this is in line with the tip. Here the tip feels a force due to the stray field and the tip is attracted to or repulsed to the surface.

With MFM measurements the  $z$ -component of the stray field is measured, which is parallel to the direction of the magnetization of the MFM tip. A disadvantage of the indirect measurements is that there are multiple possibilities to interpret the measurements of MFM. An example is shown in Fig. 20. Here in- and out-of-plane magnetization shows a similar outcome.

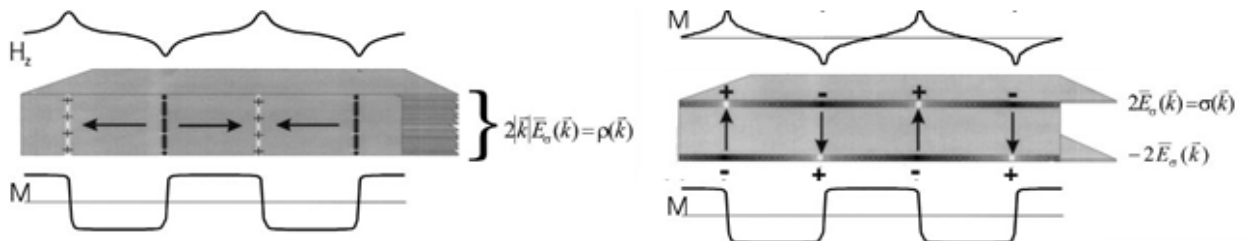


Figure 20: An in-plane and out-of-plane magnetization with both a similar stray field [14].

### 3.3.4 THE MEASUREMENTS SETUP

For the MFM measurements an AFM is used from Veeco. This AFM has an option for MFM measurements. For the MFM measurements Co-coated (SC-35-M) and Ni-coated (SC-35-LM) tips are used. The difference between the two is that the Nickel coated tips are more sensitive. After strong disturbance in the measurements, the switch was made to the Nickel tips. Both tips are fabricated by SmartTip BV in Enschede.

To characterize the magnetic characteristics of the cobalt layers, a magnetic field is applied. Two magnetic sources were used, a weak electromagnetic field applied by a coil and a strong magnetic field from a hard magnet. The field of the coil could be applied during the measurements of the tips with MFM. This could be done by placing the sample between the two field conductors.

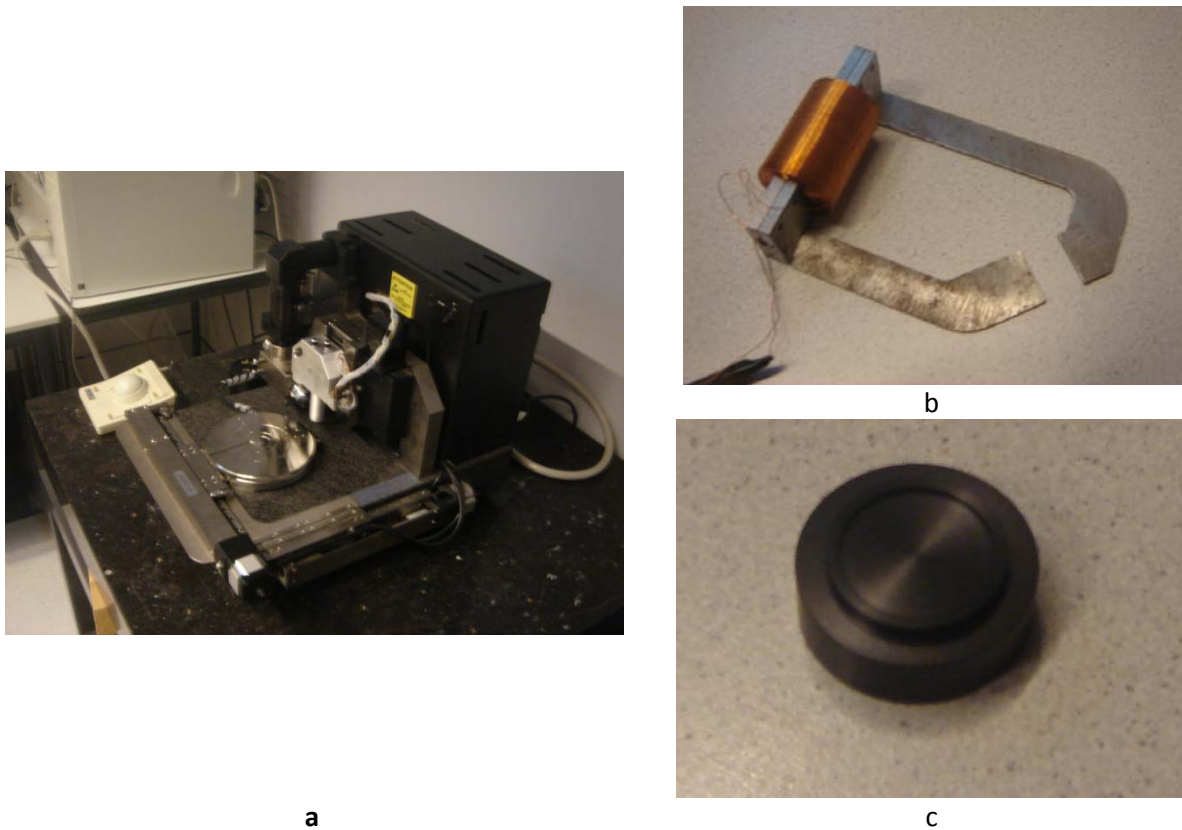


Figure 21: a) The AFM used in this assignment. b) Electromagnetic coil to apply field during measurements. c) Hard magnet to apply stronger field

### 3.3.5 VIBRATING SAMPLE MAGNETOMETER

To measure the anisotropy in a magnetic layer a vibrating sample magnetometer (VSM) is used. A schematic overview is shown in Fig. 22. The sample is mounted on a vibration unit and is exposed to a magnetic field, provided by an electromagnet. Due to the vibration of the sample emanating magnetic flux changes can be measured as an induction voltage signal by the detection coils. The magnet can be turned 180° and there are two sets of detection coils. The two sets of coils enable measurements on the flux of the magnetic moment parallel to the magnetic field and perpendicular to the magnetic field (The sample can be mounted in two different positions, horizontal and vertical, so it is possible to measure the magnetization in all directions).

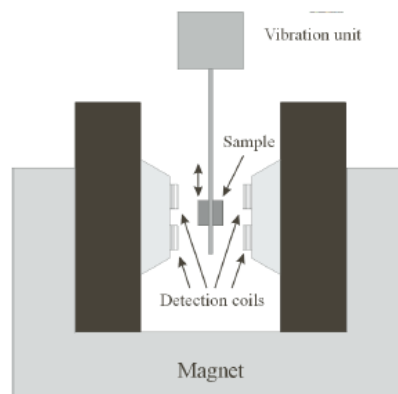


Figure 22: Schematic overview of a VSM [15].

## 4. RESULTS AND DISCUSSION

### 4.1 TIP FABRICATION

For the fabrication of the tips, the method described in the Materials and Methods section is used, and a more detailed recipe is included Appendix B. In this section some of the shape determining steps of the process are reviewed, which are essential in the fabrication process.

#### 4.1.1 DEFINING THE SHAPE OF THE CONICAL APEX

An important step to determine the conical apex of the tip in the process is the silicon etching in a KOH + IPA bath. The goal is to keep a  $1\mu\text{m}$  connection between the pyramid and the nitride cap. To control the etch process, the wafer could be checked under the microscope several times. If the wafer is taken out of the KOH bath, it should be rinsed. Otherwise KOH stains could form at the wafer and these will destroy the tips at the wafer. Another negative point of the microscope check is that silicon oxide can form at the wafer. This means that if the wafer is put back in the KOH a thin layer of oxide should be etched first. Due to a large difference in etch rate between silicon and silicon oxide, it should be taken in account that it needs a moment before the etching of the silicon continues. The moment when the etching of the silicon continues can be observed, because the gas rate is increased dramatically.

After the first test, it seemed that the first check could be taken after 20 minutes. At this time there should be a large enough connection remained between the silicon pyramid and the nitride cap. In Fig. 23 snapshots taken by a microscope are shown. The first image shows the silicon nitride cap, as it was defined by the RIE. Around the nitride cap in this image there is still silicon oxide, but just before the KOH etch this silicon layer is removed by a BHF dip. After 20 minutes the first underetching of the silicon is visible. Here an orange circle becomes visible in the centre of the blue circle. The blue circle is the nitride cap and the orange circle is the place where there is still a connection between the cap and the tip. This spot has a hexagonal shape, which is caused by the isotropic etching. Around the circle the base of the pyramid becomes visible.

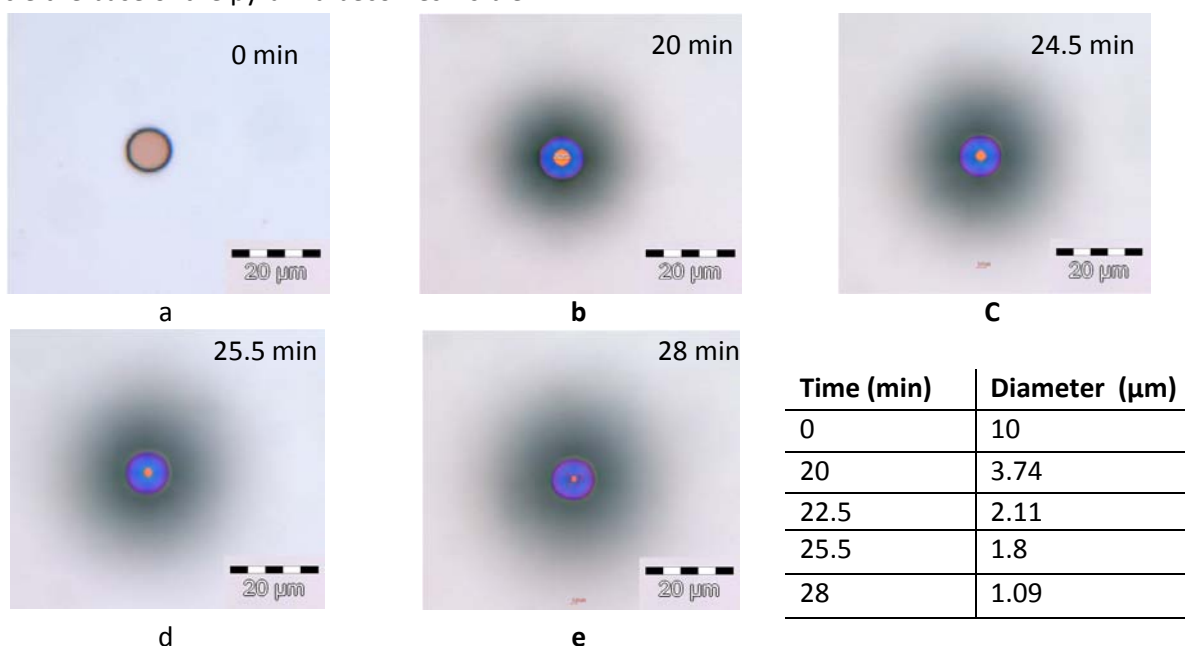


Figure 23: KOH Etching process. The process during etch time is observed by the microscope. The orange circle is the connection between the cap and the tip and the blue circle shows where the silicon is underetched.

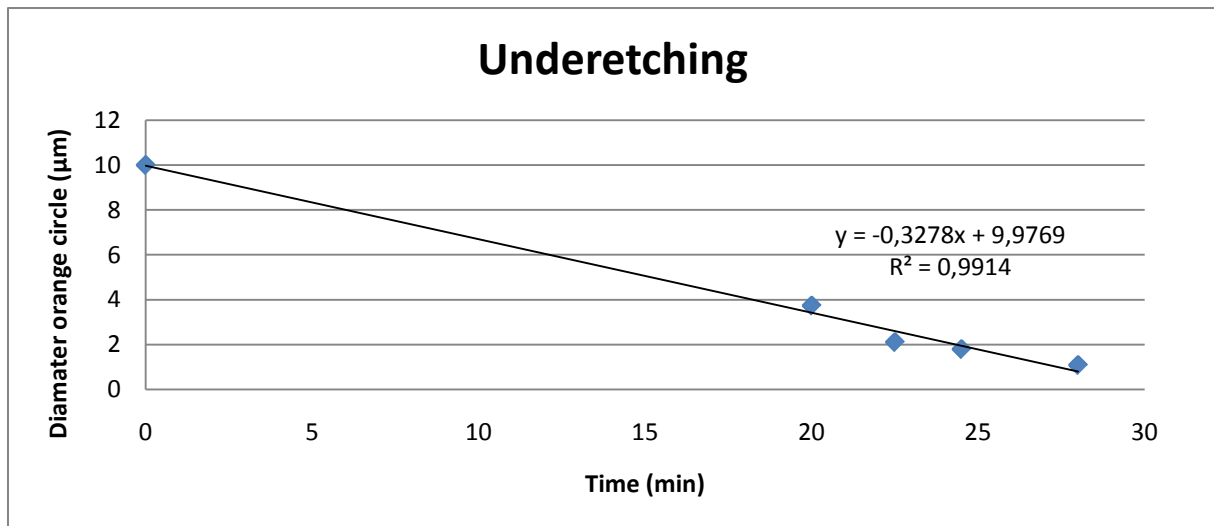


Figure 24: Diameter of the cross section of the connection between the silicon tip and the nitride cap.

The diameter of the underetch is measured at five different moments. By plotting the diameter vs. time the etch rate of the silicon in the KOH bath could be determined at  $0.33 \mu\text{m}/\text{min}$ .

The next step was a LOCOS step for the sides of the pyramid. The aim was to grow a 300 nm thick silicon oxide layer at the sides. This thickness of oxide layer is an important property, because due to diffusion of oxide under the nitride cap, the tip of the silicon pyramid should be rounded during this step. By information of the process done by Iván there it was decided that an oxidation step of 8 hours at  $1100^\circ\text{C}$  should be sufficient to form the round shape at the conical apex of the pyramid. Measurement by the ellipsometer showed after the LOCOS a silicon oxide thickness of the aimed 300 nm. After the oxidation step the microscope is used to inspect the tips with their silicon caps. Curling of the nitride cap is shown in Fig. 25. Here the cap is still connected to the pyramid. By focusing the microscope a bit lower there can be watched through the cap of the pyramid. Here four lines which are the sides of the pyramid are visible, so it seemed that the isotropic etch succeeded.

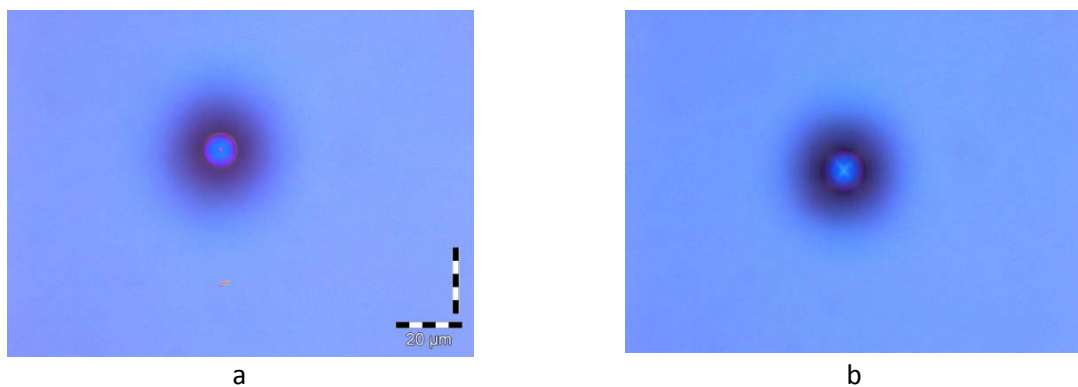


Figure 25: Optical microscope images of the tips after the LOCOS step.

After the oxidation of the pyramid, the next step was to remove the cap of the pyramid. This was done by hot  $H_3PO_4$ . There was no intention to do electrical measurement with these small tips; therefore the all the oxide was removed of the silicon pyramids. In the case of electrical measurements it is possible to remove only the oxide layer at the conical apex of the tip. In this way it is possible to regulate the size of the conducting interface between silicon and the metal layer stack. To analyze the results of the fabrication process, AFM measurements were done at several tips. As comparison also one of the double tips made by Ivan is measured. Profile measurements showed that the tips of wafer 1 were not as sharp as the tip of Ivan, but two of the three tips of the wafer 2 had the same curvature as the double tip. These tips have a curvature radius of about 500 nm.

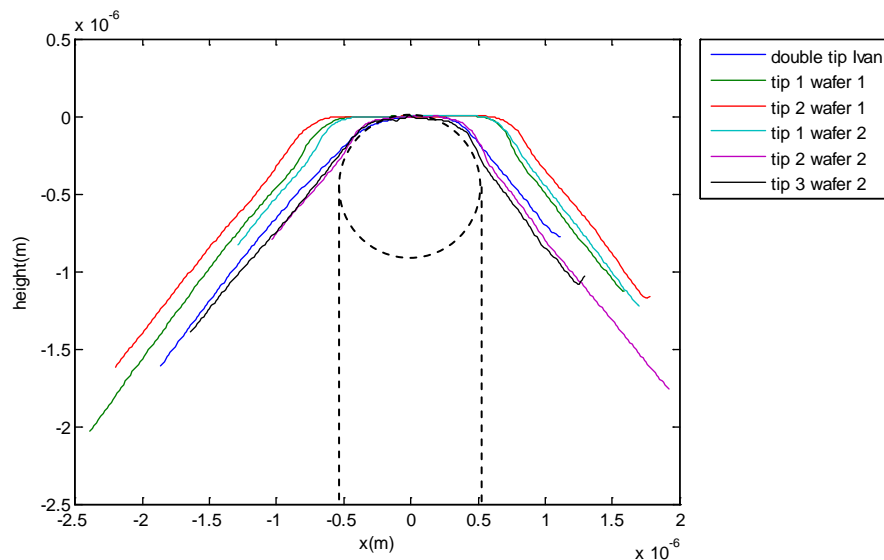


Figure 26: Profile of some of the tips of the two wafers, compared to one of the SF-STM.

### 4.1.2 EVAPORATION VS. SPUTTERING

The magnetic layer stack can be deposited with two different methods. The first option is e-beam evaporation, which is done by the DCA. Second possibility is thermal evaporation, which can be done by Sputterke. With both methods it is possible to use a gold and cobalt target during one deposition run. So it is possible to deposit the metal layer stack without breaking the vacuum environment and so getting the risk off oxidation of the cobalt. The two methods can be distinguished by the evaporation angle of the metals. In the case of Sputterke, the metal cloud is unidirectional and so there is no angle which can have an influence at the metal layer stack. In the case of the DCA, the evaporation is done under an angle, which results in a slight derivation in the thickness at the pyramids. To prevent this derivation across the pyramid the sample holder can be rotated during the evaporation.

In the thermal deposition process the aimed thickness of the metal layers are calculated by known rates and ratio's compared to each other for the different metal targets. The calibrated rate for the sputtering of gold is between the 45-50 nm/min. This rate is important to known for the deposition for the two gold layers in the metal layer stack, which thicknesses have to be respectively 10 nm and 5 nm. The sputter time of the first 10 nm gold layer take as 13 seconds and the capping layer has a deposition time of 6 seconds.

## Controlling the magnetization at the conical apex of a multi-terminal STM probe

The evaporation rate for cobalt is not standard calibrated itself. It is known that the evaporation rate for cobalt compared to the rate of gold is 0.58 : 1.76. So the rate of gold, divided by 3 will give the rate for the sputtering of cobalt. If the cobalt speed is calculated out of the rate for the sputtering of gold, the rate for the cobalt will lay between the 14.7 -16.3 nm/min. The targeted thicknesses for the cobalt layers were around the 3 nm and 4 nm. This resulted in a sputtering time of around the 15 seconds.

The two methods are analyzed by scanning electron microscopy (SEM) and MFM. By SEM it seemed that both layers showed a fully closed metal layer stack. The magnetic layer deposited on the pyramids by evaporation seems to be a closed layer. In the case of the sputtered layer, it seems in the MFM that the cobalt layer is not fully closed. The domains in the case of the evaporated layer seem to be larger.

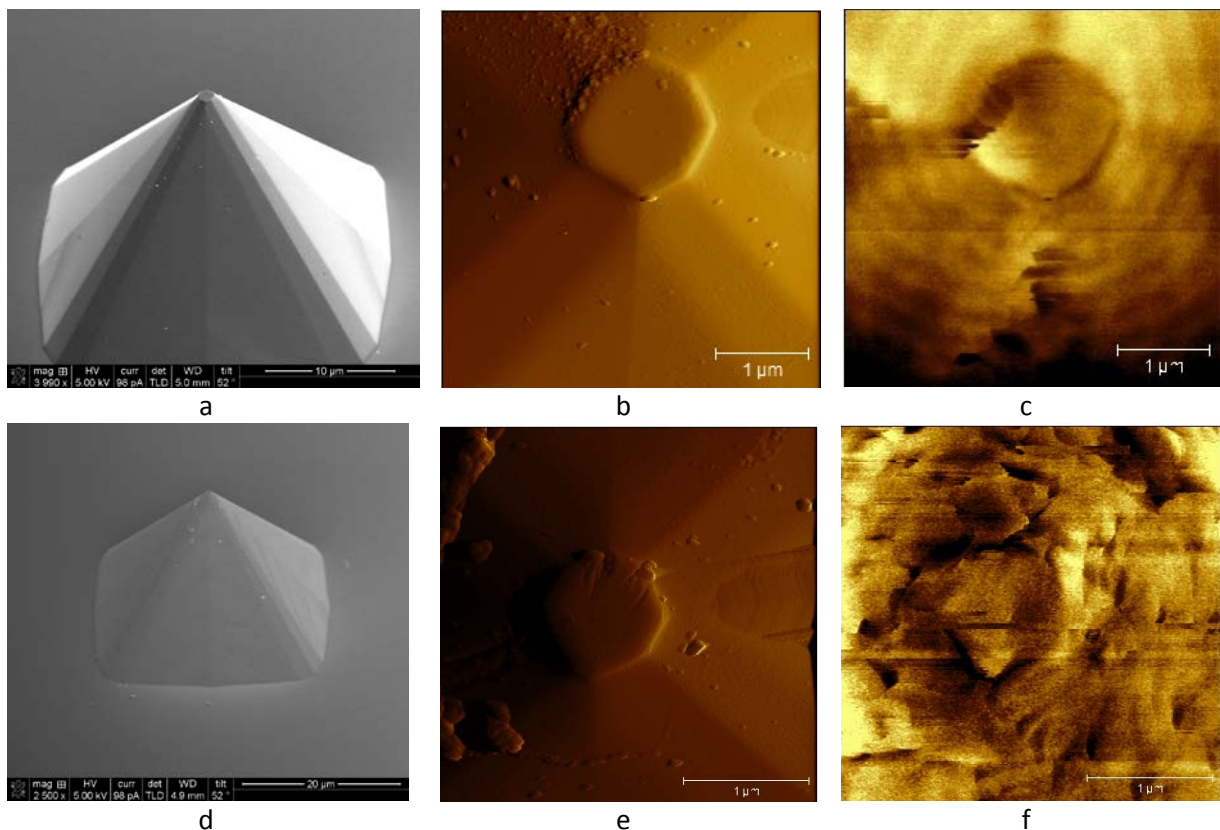


Figure 27: Comparison is shown between evaporation by DCA and sputtering by Sputterke. The magnetic signal images and their corresponding amplitude images are compared for the two deposition techniques.

### 4.2 CHARACTERIZATION OF THE MAGNETIZATION IN THE CONICAL APEX

#### 4.2.1 MEASUREMENTS AT THE DOUBLE TIP PYRAMID

The first measurements were performed a double tip made by Iván Vera Marún. This pyramid is used to define the problem with the magnetization. In Fig. 28 one of the measurements is shown of the magnetic images. There are rings visible in the image, which are caused by interference of the laser at the pyramid. This interference is only visible in the magnetic force measurements. The measurement showed a possible out-of-plane magnetization in the conical apex of the tip. It seems that in the conical apex of tip the field is come out of the conical apex. This is comparable with earlier measurements by Ivan.

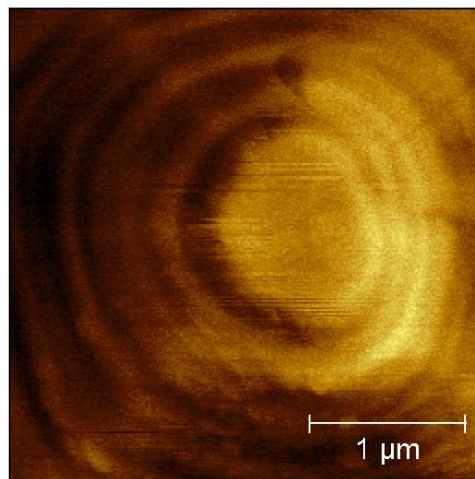


Figure 28: MFM measurement of the double tip of Ivan.

#### 4.2.2 MEASUREMENT AT A SMALL PYRAMID.

The first measurements were done at the small tips with a 3 nm and 4 nm cobalt layer. By these measurements the influence of the cobalt thickness at the magnetization is analyzed. To characterize the magnetization of the tip, a magnetic field is applied during the MFM measurements. By this it is possible to get an in-plane magnetization in the conical apex of the tip.

The measurements began with a scan under an applied field. Then the magnetic field was removed and a scan is made to analyze the remanence of the magnetization. Next the magnetic field was applied in the opposite direction to see if the magnetization could be rotated.

First the 3nm tips were characterized by the MFM. In Fig. 29 these measurements are shown. During the measurements in Figs. 29a and 29c a magnetic field is applied. The direction of the applied field is shown in the measurements. In Fig. 29a a magnetic field is applied from the bottom to the top of the image. In Fig. 29b there is no magnetic field. The measurement in 29c is made with a magnetic field applied from the top to the bottom of the image. By applying a magnetic field in the measurements four domains are measured. Three magnetic domains lie around the conical apex and a single domain is formed at the conical apex of the tip. The domain walls are marked with red lines.

Under the applied magnetic field the magnetization at the conical apex seems to be directed parallel to the magnetic field. In the tip of the conical apex a light and a dark spot becomes visible, where in the case of the light spots the magnetic field lines are coming out of the magnetic layer and in the dark spot the field lines going in the magnetic layer. If then the stray field is drawn in the

measurements, the stray field is going from the light to the dark spots. White arrows show the observed stray field. The magnetization of the magnetic layer is opposite to the stray field, which meant that the magnetization in tips is going from the dark to the light spots. So with a magnetic field it is possible to get an in-plane magnetization in conical apex of the tip. By applying the field in the other direction, the in-plane magnetization is also switched its direction, see Fig. 29c. If the field is removed, as in Fig. 29b, the in-plane magnetization of the tip disappeared and an out-of-plane magnetization is measured, which is comparable with the measurements at the double tip.

If the magnetic domains are analyzed around the tip, under an applied field a magnetic vortex around the conical apex becomes visible. The vortex changes its direction if the magnetic field is applied in the opposite direction.

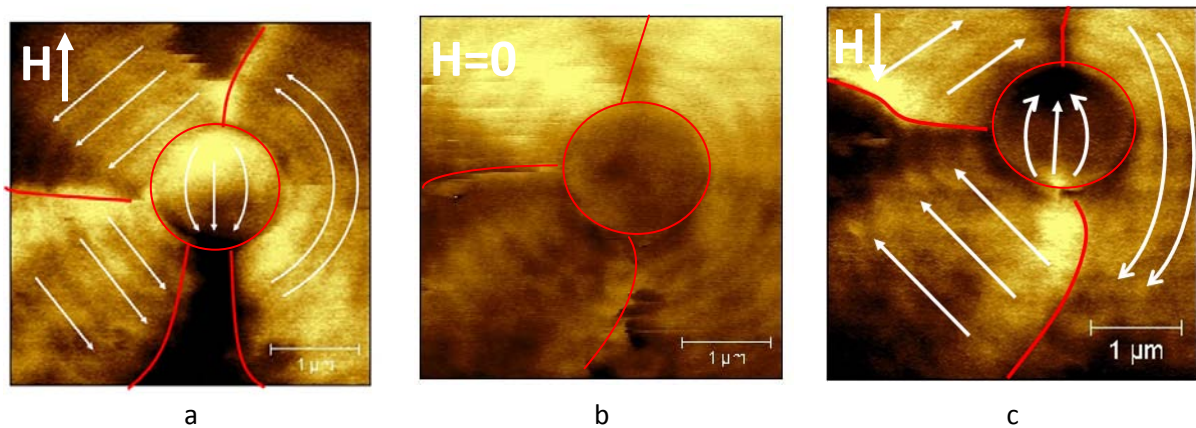


**Figure 29:** MFM measurements at a tip with a 3 nm cobalt layer. Red lines marking the domain walls and the white arrows represent the stray field. a) Measurement done under an applied field. B) Magnetic remanence measured without field. C) Measurement with an opposite applied field.

Next to the measurements of the tips with a 3nm cobalt layer, the same measurements were done at a tip with a 4nm thick cobalt layer. The measurements are shown in Fig. 30. These measurements show a similar magnetization for the applied magnetic field. An in-plane magnetization at the conical apex of the tip is visible under an applied magnetic field. As in the measurements at the 3 nm cobalt tip; the in-plane magnetization disappeared when the magnetic field was removed.

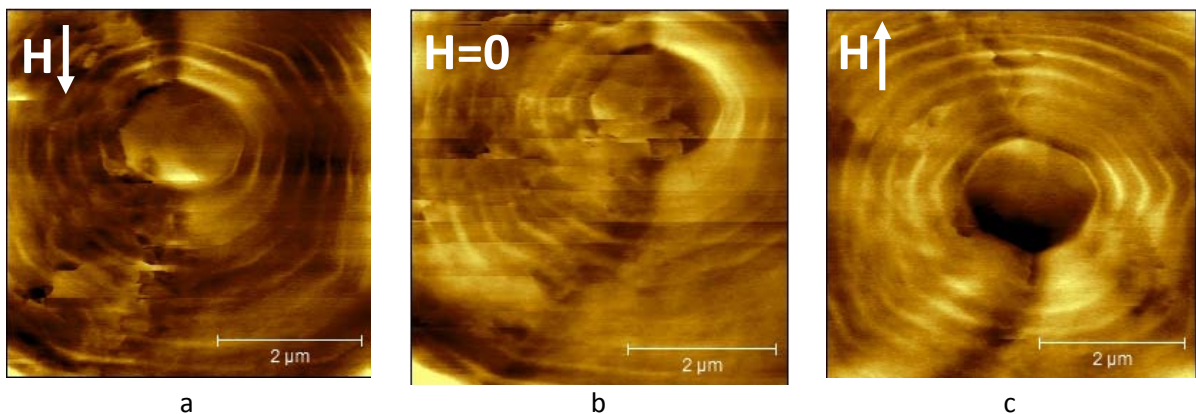


**Figure 30:** Measurements made of tips with a 4nm cobalt layer.

The measurements at the small tips show a clear in-plane magnetization under an applied field, but if the field is removed the magnetization disappeared. This corresponds with the measurements done at the double tip. A slightly change in thickness, did not show an effect at the magnetization.

### 4.3 INFLUENCING THE MAGNETIZATION DIRECTION AT THE CONICAL APEX OF THE PYRAMID.

By applying a magnetic field during the MFM measurements it was possible to measure an in-plane magnetization at the conical apex of the tip. Removal of the magnetic field resulted in the disappearance of the in-plane magnetization, which meant that the remanence of the magnetic layer was not strong enough. To increase this magnetic remanence the aim is to introduce anisotropy in the cobalt layer. Two different methods are used, which are evaporation anisotropy and shape anisotropy. Evaporation anisotropy is done by applying a magnetic field during the evaporation of the metals in the DCA. To introduce shape anisotropy in the cobalt layer, the FIB will be used to shape the metal layer stack in a strip.

#### 4.3.1 EVAPORATION ANISOTROPY

To introduce evaporation anisotropy in the magnetic layer, during evaporation in the DCA a magnetic field was applied. This is done by magnets at the sample holder. The field direction applied by the magnetic field is shown in Fig. 31 as  $H_{DCA}$ . The magnetic field is applied during the deposition process, so it is also present during the evaporation of the gold layers. Either no effect is expected at the gold, because it is a paramagnet. The field only contributes to the anisotropy during the evaporation of the cobalt layer. During the evaporation the sample was rotated. Due to this there will be a uniform layer thickness at the tips.

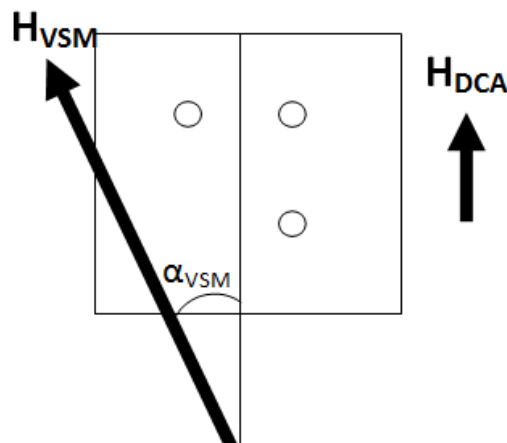


Figure 31: Setup of the sample in the VSM.  $H_{DCA}$  shows the direction of the magnetic field during the evaporation of the metal layers on the silicon pyramids.  $\alpha_{VSM}$  is the angle between the magnetic field of the VSM ( $H_{VSM}$ ) and  $H_{DCA}$ .

VSM measurements are done to determine the easy-axis in the cobalt. This is done by measuring the hysteresis loops of the magnetic response. By doing these measurements under different angles  $\alpha_{VSM}$  to the applied magnetic field  $H_{VSM}$ , the preferable magnetization of the cobalt film can be determined. The angle compared to the sample orientation is shown in Fig. 31. If angle  $\alpha_{VSM} = 0^\circ$ , the field during the VSM measurements is parallel to the  $H_{DCA}$ . The angle of the measurements is varied between  $-90^\circ$  and  $90^\circ$ , with steps of  $10^\circ$ . This should give enough points to see the preferable magnetization direction of the magnetic field. The field is swept during the measurements between 1000 and -1000 Oe. Between -50 and 50 Oe small steps are made, to have a high resolution in the range where the magnetization direction will be switched. By sweeping the field from positive to negative and then back from negative to positive, the measurements for the range  $90^\circ$  to  $270^\circ$  are

performed if the field is swept back. So it not required to rotate the sample and do a second set of measurements to do measurements for the full 360°. All the data points are the average of ten measurements and the measurements were performed at room temperature.

Magnetic characteristics measured by VSM are shown in Fig. 32. The hysteresis loop of the cobalt film is measured, during the sweeping of a magnetic field. The shape of the hysteresis loop gives information over the behavior of the magnetic in a magnetic field. A hard magnet has a rectangular hysteresis loop and a soft magnet shows a more linear response to the applied field. Some important points in the loops are the saturation magnetization, the magnetization remanence and the magnetic coercivity. The saturation magnetization  $M_S$  is the maximum magnetization of the sample. At this value all the magnetic moments in the material points in the same direction. The remanence magnetization  $M_R$  is the magnetization if there is no applied field. This is the point where the loop crosses the 0 Oe. The magnetic coercivity  $M_C$  is the point where the magnetization switched its direction. In the hysteresis loop this is the point where it crosses the line where the magnetic moment is 0 Am<sup>2</sup>.

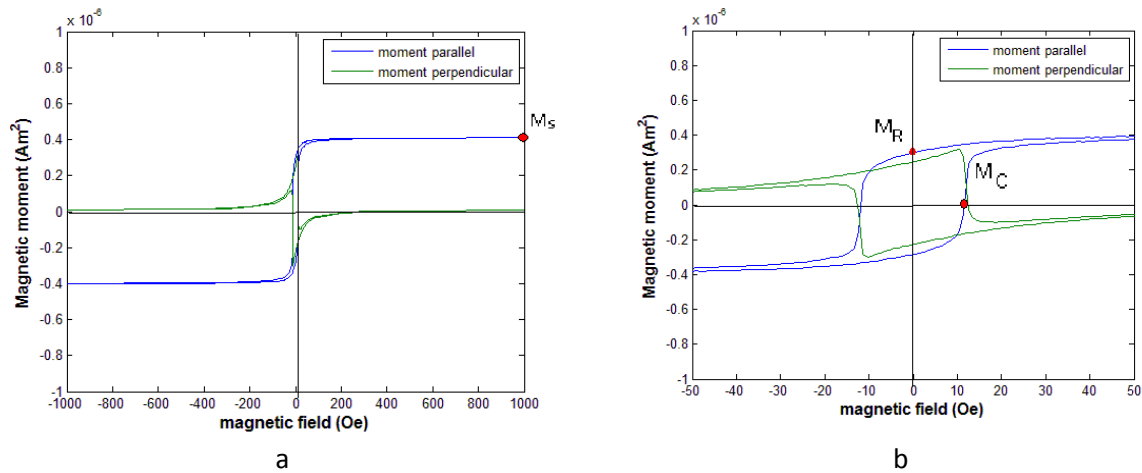


Figure 32: a) Full hysteresis loop at 40° shows the saturation magnetization. b) Zoomed-in at the hysteresis loop at 40° shows the remanence magnetization and the magnetic coercivity

To measure the effect of the evaporation anisotropy measurements were done on a metal layer stack with a 10 nm cobalt layer, which was evaporated at silicon. A few of the hysteresis loops are shown in Fig. 33. The measurements of the moment parallel to the applied magnetic field are the blue graphs and the measurements of the magnetic moment perpendicular at the magnetic field are the green graphs.

The hysteresis loop of the measurement at 0° where the applied field in the VSM is parallel to the magnetic field during evaporation shows the behavior of a hard magnet. In this case the magnetization prefers to orient in the direction of the magnetic field and the moment perpendicular is almost disappeared. If the  $\alpha_{VSM}$  is changed to -40° and 40° the hysteresis loops of the moment parallel to the applied magnetic field is decreased and the perpendicular flux is increased. For the measurements at a field angle of -70° and 70° a more soft magnetic response is measured. The hysteresis loop at a 90° angle shows an equal response for the parallel and the perpendicular moment.

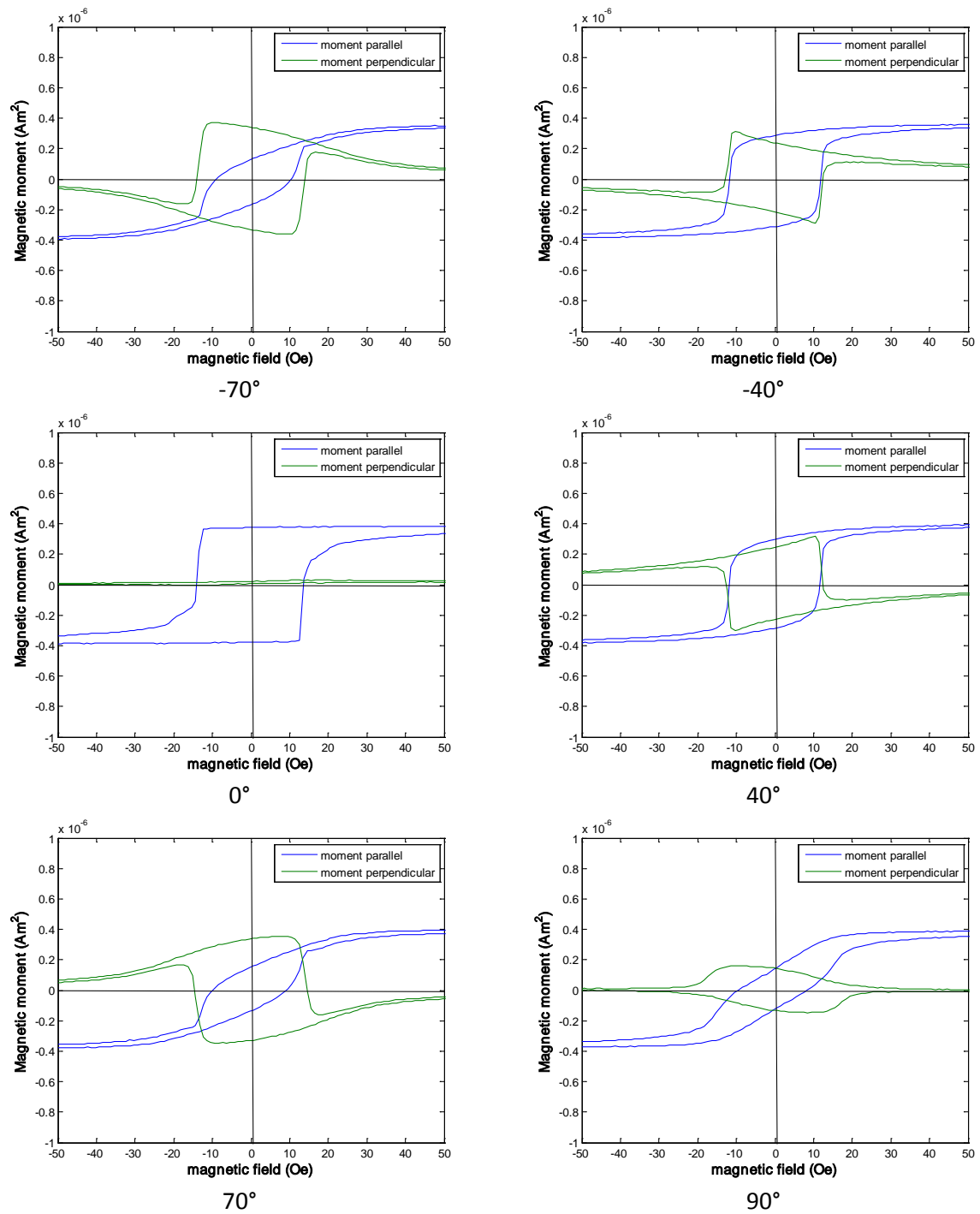


Figure 33: Hysteresis loops of the cobalt film measured by VSM under different angles.

In Fig. 34 the magnetic remanence is plotted against the angle of the magnetic field, and a uni-axial anisotropy becomes visible. The easy-axis in the magnetic layer is visible at  $0^\circ$ , which is equal to angle of the applied field during evaporation. The measurements showed that there is a possibility to introduce evaporation anisotropy by doing the evaporation under an applied magnetic field. The hard axis should be normally perpendicular to the easy axis, but in this case the hard axis seems to be at  $70^\circ$ . The signals of the parallel and perpendicular magnetic moment at  $90^\circ$  are equal.

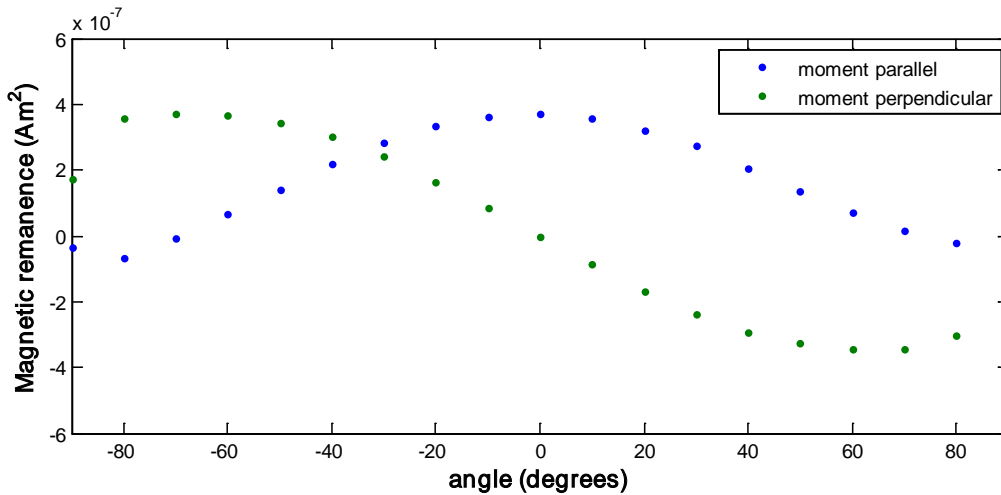


Figure 34: Remanence measurements show a uni-axial anisotropy.

To analyze the discontinuity in the sinusoidal graph at the expected angle of the hard axis, the fully  $360^\circ$  is plotted in Fig. 35. The magnetic remanence measurements for  $90^\circ$  to  $270^\circ$  are out of the data sets for the measurements of  $-90^\circ$  to  $90^\circ$ , but the magnetic remanence is used when the field is going from negative to positive field. This could be done because in this case the applied field behaves the same for if the sample is rotated  $180^\circ$  and then measuring it from  $-90^\circ$  to  $90^\circ$ . If the data is analyzed, the sinusoidal character is visible, which is characteristic for a uni-axial anisotropy. At  $90^\circ$ , which contains two measurement points, there is a discontinuity and the measurement points for the parallel moment do not follow the sinusoidal relation. For the perpendicular moment at this  $90^\circ$  there is a same discontinuity and the parallel and perpendicular moment has the same value. It seems that there is another easy axis at  $90^\circ$ .

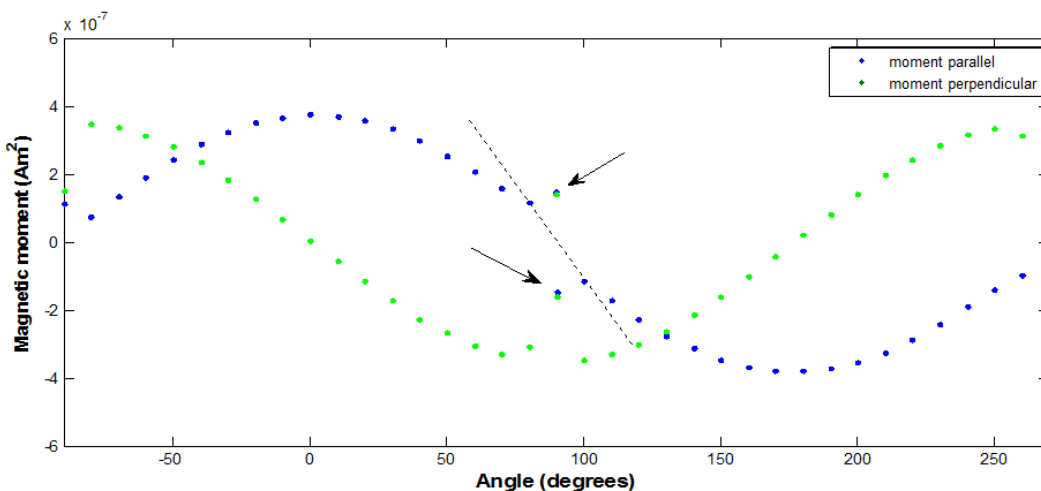


Figure 35: Full spectrum of the magnetic moment vs. the angle of the magnetic field. A derivation is visible at  $90^\circ$ .

### 4.3.2 EVAPORATION ANISOTROPY AT THE MAGNETIC PYRAMID.

The evaporation anisotropy was applied at tips with a 10 nm cobalt layer. The gold layers in the stack had the standard thickness of 10 nm and 5 nm. The magnetization of the tips was characterized by MFM. A magnetic field of the electromagnetic coil was used during the measurements. The results are shown in Fig. 36. In the images there is a strong interference of the laser at the tip visible.

When a magnetic field is applied, an in-plane magnetization in the direction of the magnetic field is visible at the conical apex of the tip. This corresponds with the measurements done at the tips with a 3 nm and a 4 nm cobalt layer. In the measurements three magnetic domains could be distinguished, which are one at the conical apex and two around the conical apex. The domain walls of these domains are marked with a red line and the stray field is marked with the white arrows. If then the magnetization in the conical apex is analyzed, both measurements show a parallel magnetization to the applied field. Around the conical apex a vortex is observed. When the magnetic field is removed, the magnetization does not disappear completely. It seems that the magnetization becomes a bit weaker as it was under an applied magnetic field, but the tip is still weakly magnetized in the direction of the magnetic field.

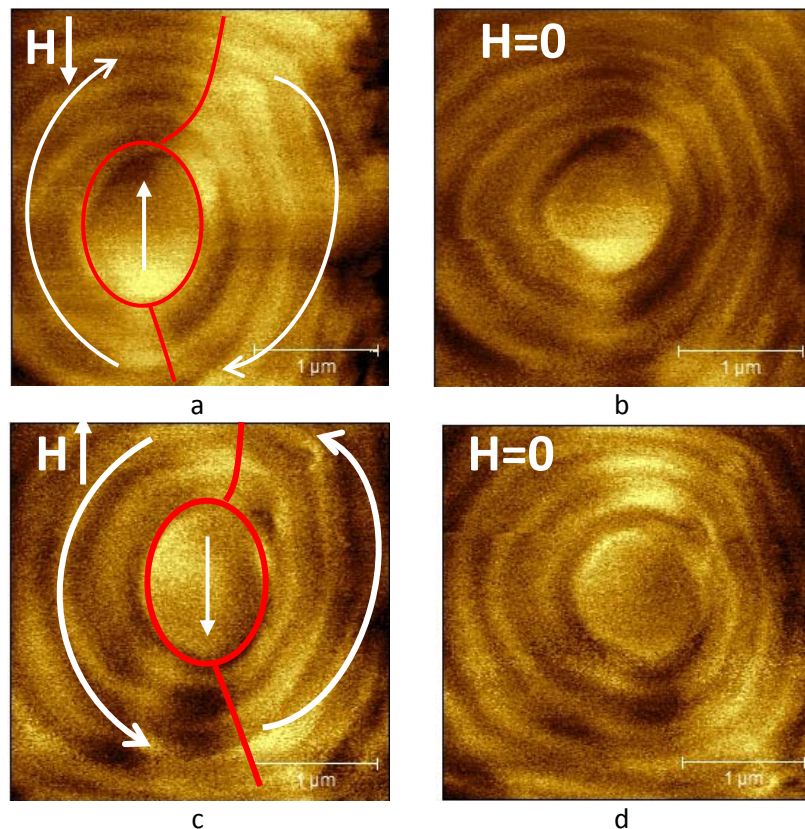


Figure 36: Measurements of the tips with evaporation energy: red lines' marking the domain walls and the stray field is indicated by the white arrows.

Measurements show that the evaporation anisotropy can be used to enlarge the anisotropy in the magnetic layer. This anisotropy is in the direction of the applied magnetic field during evaporation of the cobalt layer.

### 4.3.3 SHAPE ANISOTROPY

To look at the effect of the width of a strip and the length/width ratio, shape anisotropy is tested with rectangular shapes. These rectangular strips were made by the focused ion beam (FIB) in a 10 nm cobalt layer, sandwiched by a 10 nm and a 5 nm gold layer. This metal layer stack corresponds with the layer stack used at the tips. This layer stack is evaporated at a silicon substrate, and during the evaporation the sample is rotated.

The lengths and widths are varied to see the effect of differences in lengths and widths and so different length/width ratios are characterized. In Fig. 37 an SEM image with the FIB'ed raster is shown. The aim was to FIB 60 nm deep lines, and at the cross points the depth is 120 nm. This to be sure that the metal layer stack will be etched completely, so that there is no magnetic connection between the strips will remain after the FIB.

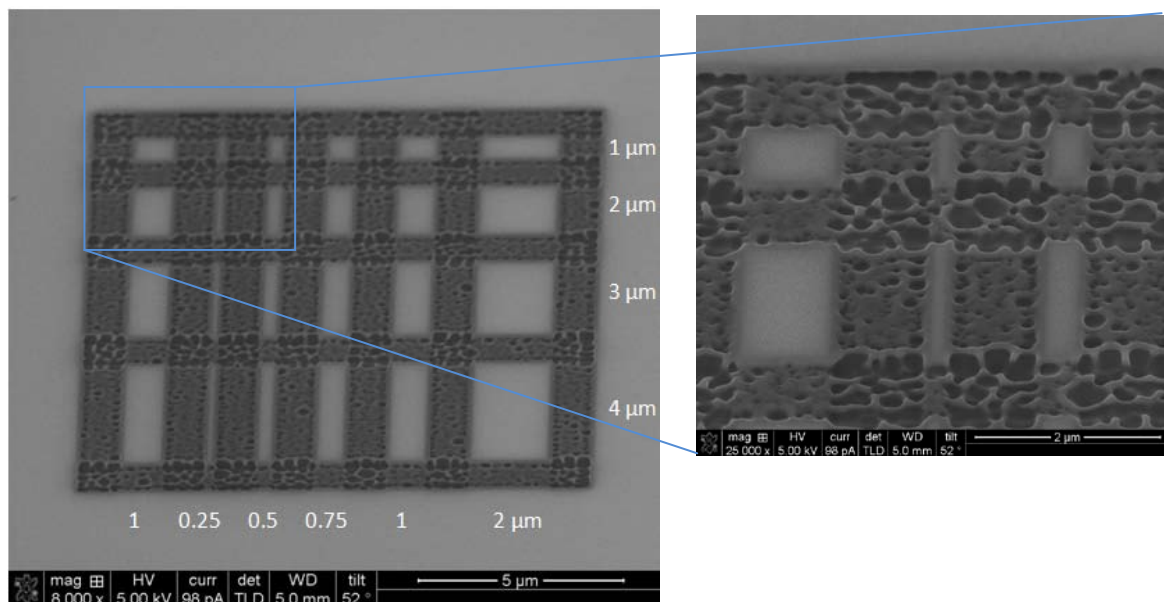


Figure 37: An overview of the Fib'ed strips with the widths and lengths in a 10 nm thick cobalt layer.

The magnetization of the strips is characterized by MFM. During the first MFM measurements, the field of the electromagnetic coil is applied to force the magnetization in the direction of the field. The results in Fig. 38 show that the magnetization in all the strips with a width of 1 μm and 2 μm switched in the direction of the applied magnetic field, but the strips with a smaller width could not be switched by the applied field. The strips with a 750 nm width and a 1 μm and 4 μm length did switch, but the strips with the same width but, a 2 μm and 3 μm length did not switch. Strips with a width of 500 nm could not be switched by the applied field. Strips with 250 nm width did not show any magnetization.

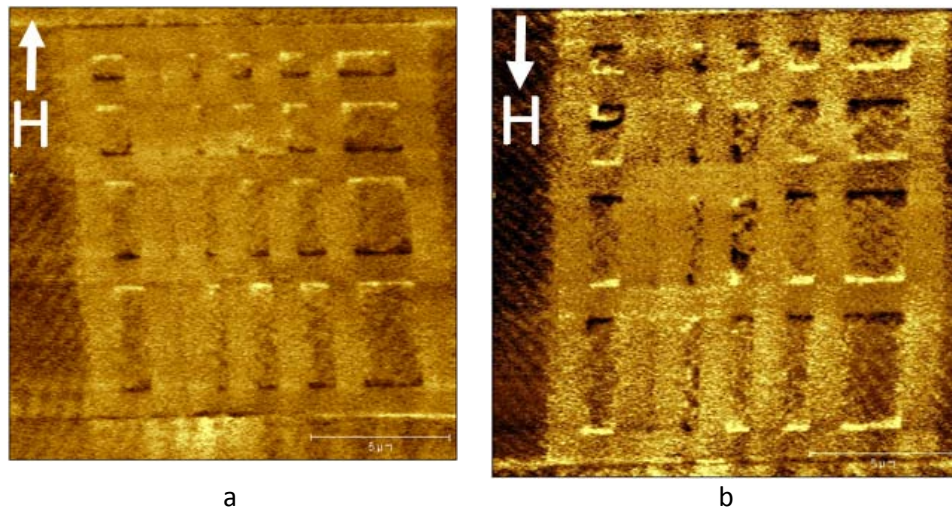


Figure 38: Measurements of the strips under an applied field of the electromagnetic coil.

To characterize the coercivity and the remanence of the strips, the stronger field of the hard magnetic used to magnetize the strips. Results are shown in Fig. 39. With the stronger field it was possible to switch the direction of all the strips.

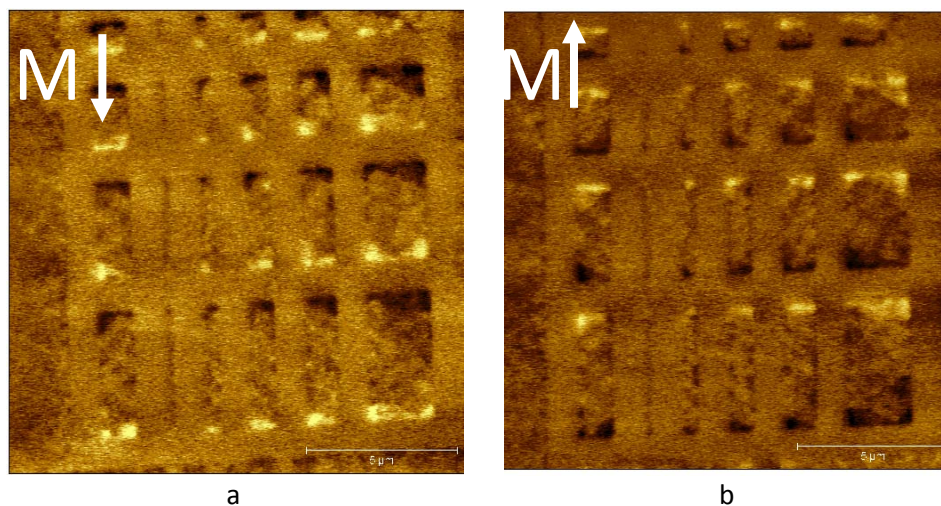


Figure 39: Measurements of the strips after magnetization with a strong magnetic field.

The shape anisotropy is also characterized with a magnetization direction perpendicular at the strips. The characterization by MFM was done after the magnetization, so there was no field applied during the measurements. The results are shown in Fig. 40. The strips with widths of  $2\ \mu\text{m}$  could be magnetized parallel to the applied field. In the strips with widths of  $0.5$  to  $1\ \mu\text{m}$  the magnetization of the strips showed a more complex situation. Some magnetizations are directed to the magnetic field, but in films with a longer length, and so a larger length/width ratio there are strips which are not magnetized parallel to the applied field. Strips with a length of  $4\ \mu\text{m}$  and a width of  $1\ \mu\text{m}$  are magnetized along the length of the strips. It seems that the easy-axis lies in the length of the beam. In the  $4\ \mu\text{m}$  strips with widths of  $0.75$  and  $0.5\ \mu\text{m}$  no uniform magnetization is measured and the magnetization shows small domains.

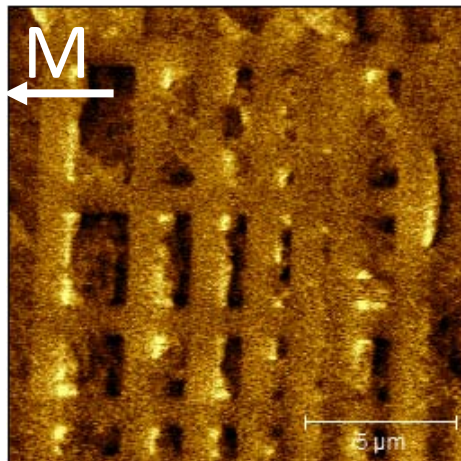


Figure 40: Measurements of the strips with a perpendicular magnetization.

The measurements at flat strips show that a rectangular shape can be used to introduce anisotropy in the magnetic layer. A high length/width ratio increased the remanence and coercivity of the strips.

### 4.3.4 SHAPE ANISOTROPY AT THE PYRAMID

To introduce shape anisotropy to the pyramid the FIB is used to shape the metal layer stack into a strip. The depth was 100 nm, which was done to be sure that the magnetic cobalt layer was removed completely by the FIB. In that case there was no connection between the side of the strip and the rest of the magnetic layer. The strip still had a connection with the magnetic layer at the bases of the tip. These contacts are needed for to contact the metal layer stack at the tip. In Fig. 41 an example of one of the strips at the tip is shown. The zoomed image shows the edge of the strip. There is a clear difference visible between the metal layer stack and the FIB'ed area. The metal layer stack seems to be intact and it seems that at the FIB'ed area the metal layer stack is removed.

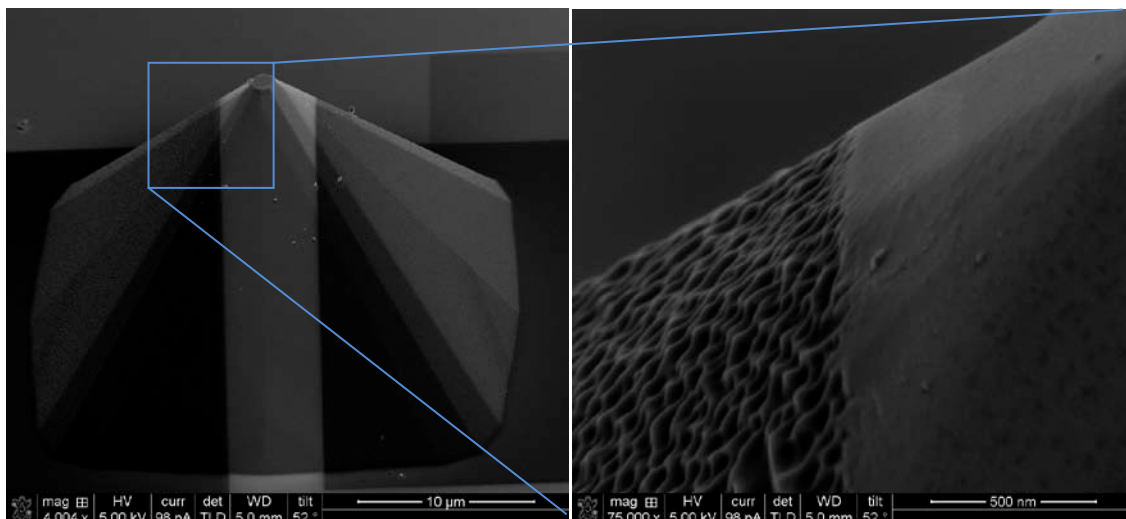


Figure 41: Overview of one of the strips at the pyramids, with a close up at the edge of the strip

To analyze the effect of the strip at the magnetization on the tip, different strips are characterized by MFM. Different widths are made to change the length width ratio of the strip. The importance of this parameter is shown in the measurements with the magnetic strips. Strips, with widths of 1  $\mu\text{m}$  and 8  $\mu\text{m}$  have been made by the FIB at the pyramids. The length of the strips is around the 40  $\mu\text{m}$ , which results in a ratio of 5:1 and 40:1.

### MAGNETIC DECOUPLING AT THE SIDES

The first two magnetic strips had a width of 8  $\mu\text{m}$ . These strips were made on pyramids with a 4 nm cobalt layer. Measurements done at the pyramids before the FIB process can be found in chapter 4.2.2. These measurements show that under a magnetic field it was possible to get in-plane magnetization, but when the magnetic field was removed, the magnetization switched back to out-of-plane magnetization. At the first tip the largest part of the metal layer stack was removed by the FIB, only the strip was left at the tip. An SEM image is shown in Fig. 41a. At the second tip, the FIB'ed area was made smaller, which is shown in Fig. 41b. By changing the area of the FIB'ed part, the effect of the stray field at the sides of the strip and the rest of the magnetic layer is analyzed. If there is a strong coupling between the magnetic strip and the rest of the magnetic layer by the stray field, it will be necessary to remove a large part of the metal layer stack, as in Fig. 42a.

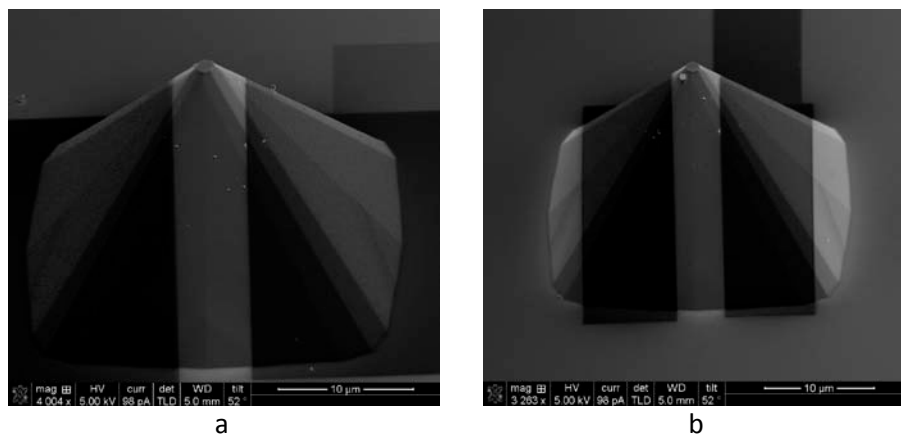


Figure 42: SEM images of two images with a different FIB area. a) A large FIB area. b) smaller FIB area.

The MFM measurements of both strips are shown in Fig. 43. The tips were first measured with a magnetic field directed downward. Then the magnetic field was removed to see the remanence of the magnetization. Then a magnetic field is applied in the other direction and a measurement was made. In the images the rings have their origin in the interference of the laser at the tip. By applying a magnetic field it was possible to magnetize both tips in-plane parallel to the field. When the field was removed the magnetization did not disappear completely. In both images without field, out coming stray field is measured at the bottom of the apex. It seemed that the shape of the strip brought anisotropy in the magnetic layer. Either the magnetization at the apex is not strong enough to withstand the stray field of the MFM tip. This is shown clearly in Fig. 43b. Here at the apex a magnetic switching is visible. If the magnetic field is applied in the opposite direction it was possible to magnetize the tip in the other direction.

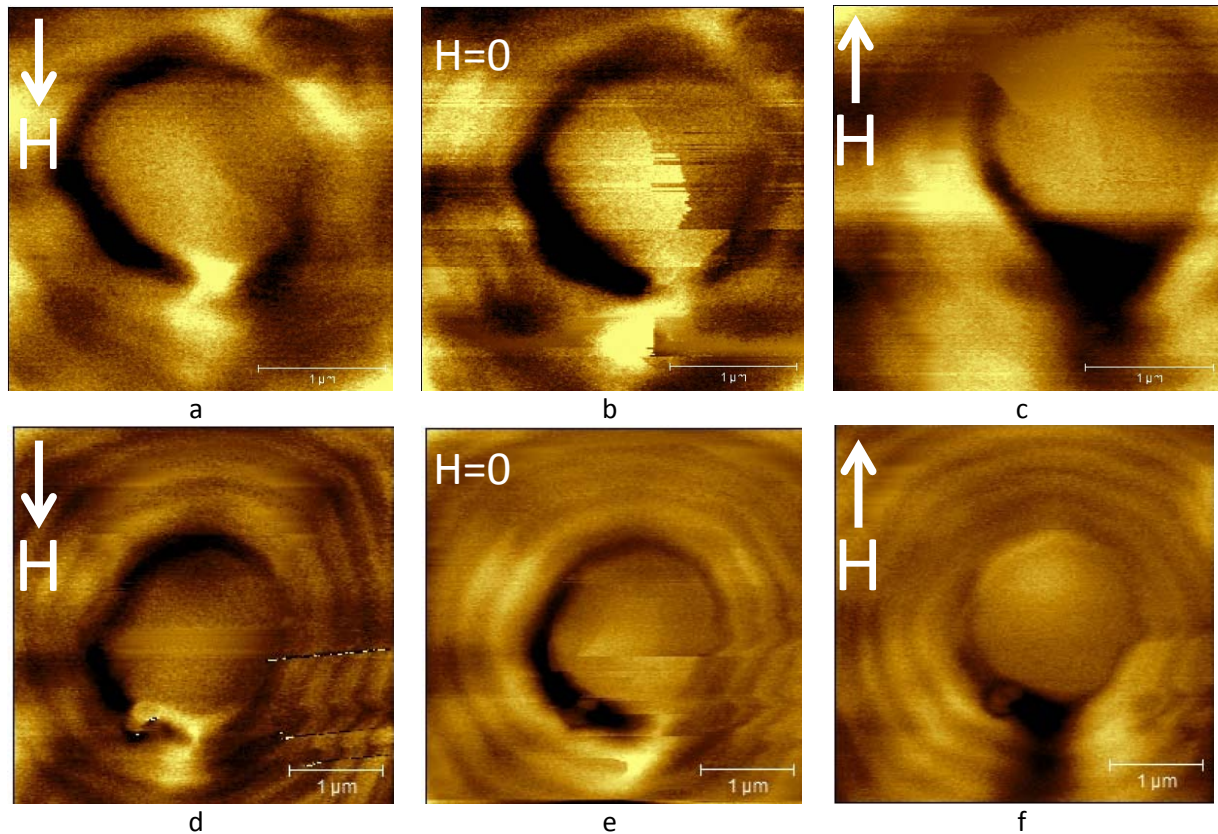


Figure 43: Measurements of the 8  $\mu\text{m}$  strips. a,b,c: strips with a large FIB area. d,e,f: tips with a smaller FIB'ed area. A field is applied to characterize the magnetization.

#### DECOUPLING THE STRIP AT THE BASE

The next step was to decrease the width of the strip to 7  $\mu\text{m}$  and to decouple the magnetic strip at the base of the tip. In the end this decoupling is not required, because there can be no conduction between the magnetic strip and the STM system. The smaller width of the strip increased the length/width ratio in the strip slightly. According to the flat strips measurements this should have a positive effect at the shape anisotropy in the magnetic layer and should increase the remanence. The used tip had a metal layer stack with a 3 nm cobalt layer. The strip is shown in Fig. 44.

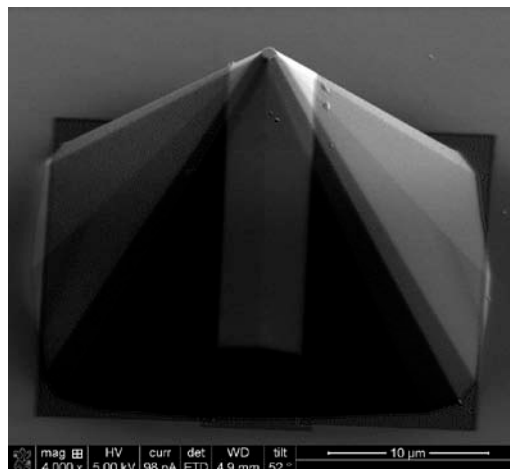


Figure 44: A decoupled strip with a width of 7  $\mu\text{m}$

Measurements were done by MFM and a magnetic field of the coil was applied during the scans parallel to the strip. The results are shown in Fig. 45. After the measurements in a magnetic field, the field was removed to analyze the remanence of the magnetization. In the measurements under an applied field an in-plane magnetization is visible.

The in-plane magnetization at the conical apex switched back to an out-of-plane magnetization after removal of the magnetic field. Either the magnetization around the conical apex of the tip did not disappear completely. A part of the magnetization at the tip remained. The magnetic remanence is visible at the darker spots around the edge of apex, a place where the stray field going into the tip. In Fig. 45b this spot is at the bottom side of the apex and it has the same shape and size as in Fig. 45a. In Fig. 45 the outgoing stray fields are visible at the top side of the apex, only in this image the contrast is not that really high. But the outgoing field lines in the measurement in this measurement are at the same place of tip as in the measurement shown in Fig. 45c. This measurement was under an applied field.

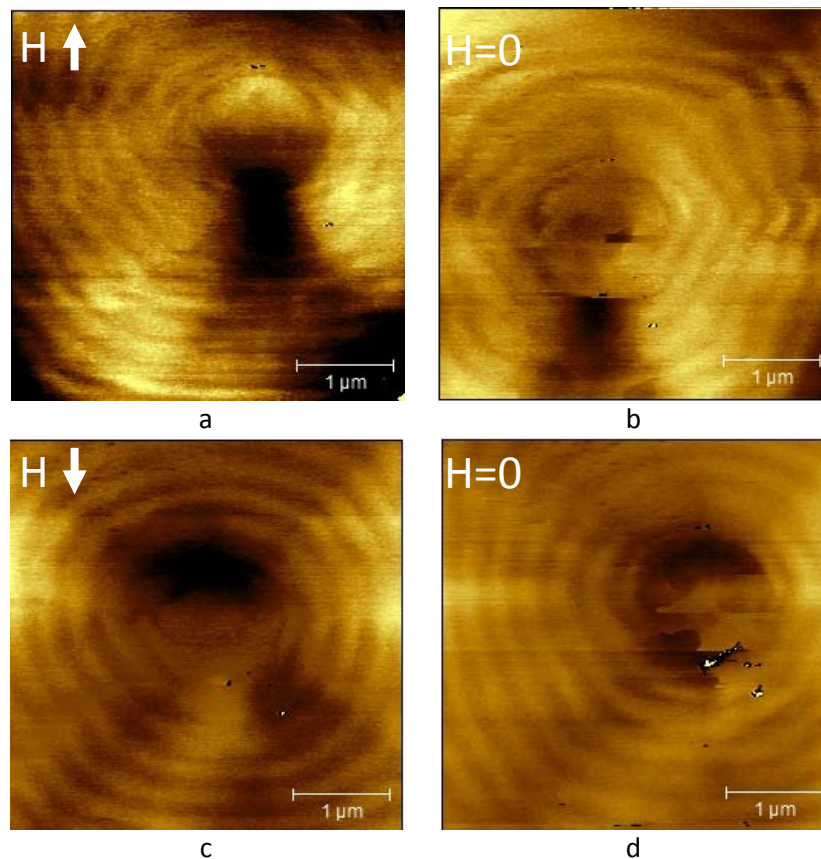


Figure 45: a and c: Measurements under an applied field; b and d: magnetic remanence after removal of the field.

### THE MAXIMUM LENGTH/WIDTH RATIO

In an effort to increase the magnetic remanence, the length/width ratio of the magnetic strip was increased. This is done at two tips; one with a strip width of 2  $\mu\text{m}$  and one with a strip width of 1  $\mu\text{m}$ . These strips are shown in Fig. 46. The metal layer stacks were deposited by Sputterke, which is the thermal evaporation technique. MFM measurements before showed a grainy magnetization of the cobalt layer, when it was made by Sputterke.

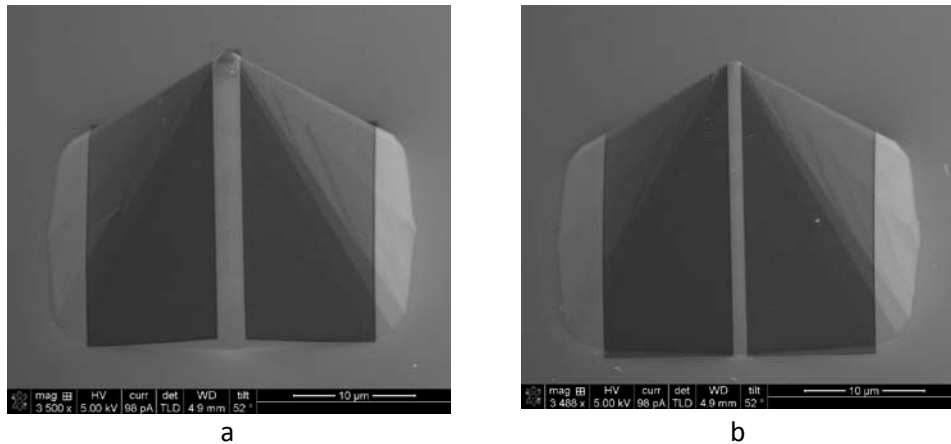


Figure 46: Strips made at two tips with a 5nm cobalt layer to increase the length/width ratio. A) Strip with a width of 2  $\mu\text{m}$ . B) 1  $\mu\text{m}$  width strip.

The tips are characterized by the MFM, see Figs. 47. Figs. 47a, 47b and 47c show the results of the 2  $\mu\text{m}$  strip and Fig. 47d, 47e and 47f shows the results of the 1  $\mu\text{m}$  strip. The field of the electromagnetic coil is applied during measurements and the conical apex of the tip was in-plane magnetized by the applied field. The tips show a more grainy magnetization of the cobalt layer, which is caused by the thermal evaporation. The conical apex of both tips could be magnetized in-plane with the magnetic field. This corresponds with the measurements at other tips.

If the field was removed, the magnetization in the conical apex of both tips disappeared. The magnetization at the conical apex showed magnetic switching, which was influenced by the stray field of the tip. Around the conical apex of the tip there is both tips one domain wall visible. The magnetization around the conical apex showed a high remanence, for example the domain wall at the top of the conical apex in Fig. 44e did not disappear when the field was switched off. The remanence of the field here was stronger than the stray field of by the MFM tip.

The magnetization of the cobalt layer is increased by introducing shape anisotropy. Measurements with several strip widths showed that a high length/width ratio increased the magnetic remanence. The increased remanence had the most influence in a higher remanence in the magnetic layer around the conical apex of the tip. In the conical apex no measurement showed an in-plane magnetization after removal of the magnetic field. Magnetization at the conical apexes showed switching, which seems to be caused by the stray field of the MFM tips.

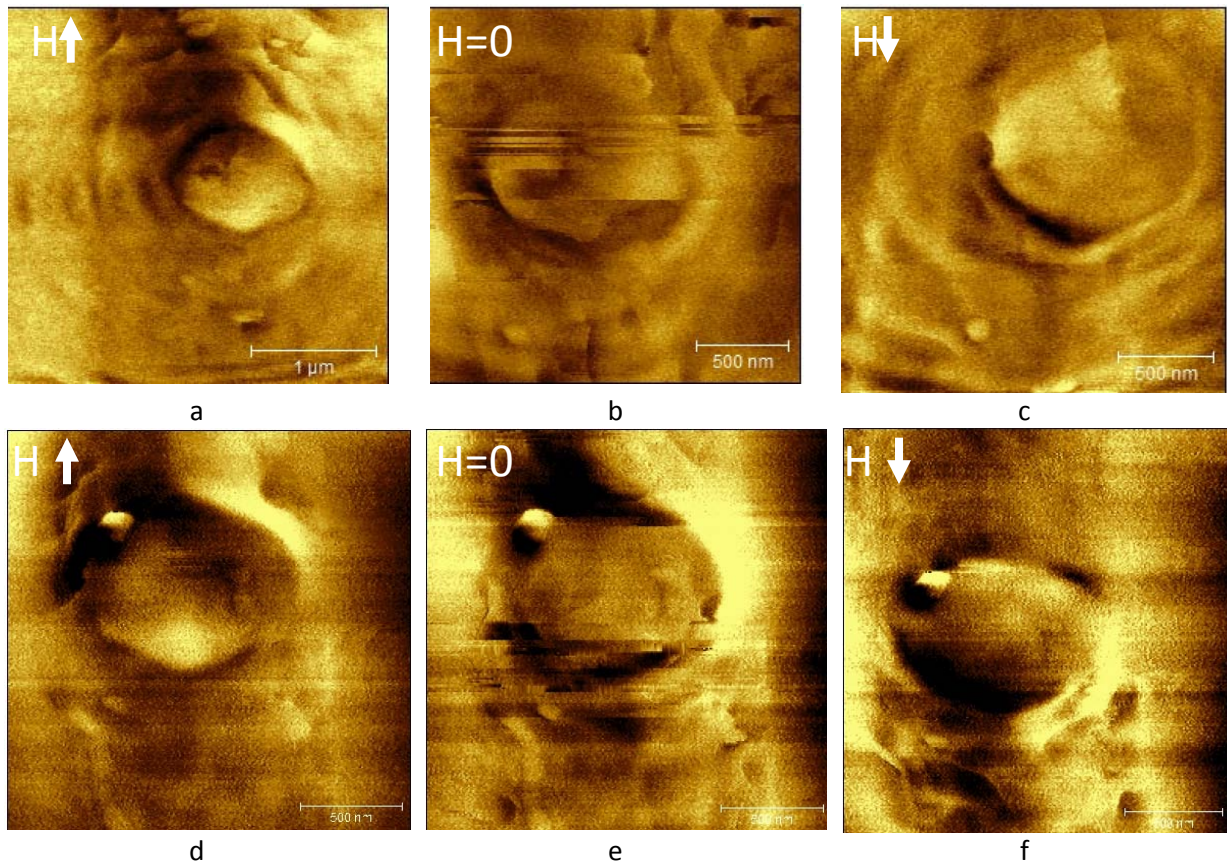


Figure 47: Measurements at tips with strips with width of 2  $\mu\text{m}$  (a,b,c) and 1  $\mu\text{m}$  (d,e,f).

#### 4.4 COMBINE SHAPE ANISOTROPY AND EVAPORATION ANISOTROPY

Two methods to enlarge the anisotropy in the magnetic layer have been introduced and both had a positive effect at the in-plane magnetization. The next step was to combine the evaporation anisotropy and the shape anisotropy. For this the same tip as in section 4.3.2 is used and at the tip a 1  $\mu\text{m}$  width strip is made. This tip had a metal layer stack with a 10 nm cobalt layer. The strip was shaped in the direction of the easy-axis measured by the VSM. SEM images of this strip are shown in Fig. 48.

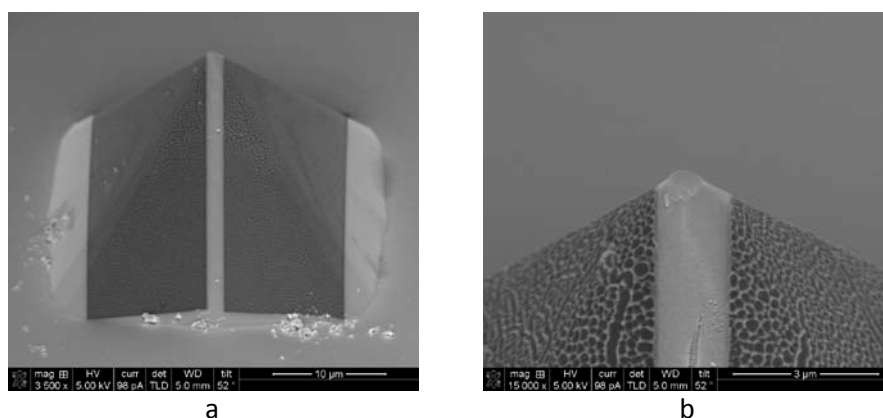


Figure 48: SEM images of the small tip with a magnetic strip of 10 nm cobalt layer. a) A complete overview of the tip. b) Zoomed image of the top of the tip.

The tip was characterized by MFM. In the measurements the tip was first magnetized with the field of the coil and a second set of measurements were done after it was magnetized by the field of the hard magnet. These results with the coil are shown in Fig. 49a and 49d. The measurements with the hard magnet are shown in Fig. 49b and 49e. In Fig. 49c and 49f the domain walls and stray field of the measurements after magnetized by the hard magnet are indicated.

Measurements under the applied field of the coil showed that the field was not strong enough to switch the magnetization of the tip. In both measurements the magnetization at the conical apex of the tip showed a parallel direction to the first applied field. By turning the direction of the field in the opposite direction, the magnetization could not be switched.

After magnetized by the stronger field of the hard magnet it was possible to overcome the coercivity and switch the direction of the magnetization. In Fig. 46b and 46e two domains are visible around the conical apex and one at the apex of the tip. The walls of these domains are marked in Fig. 46c and 46f. The stray field around the conical apex shows in both measurements a vortex. This corresponds with the vortices measured before at other tips. The domain at the conical apex of the tip shows a single domain with an in-plane magnetization, which has the magnetization parallel to the applied field during the magnetization.

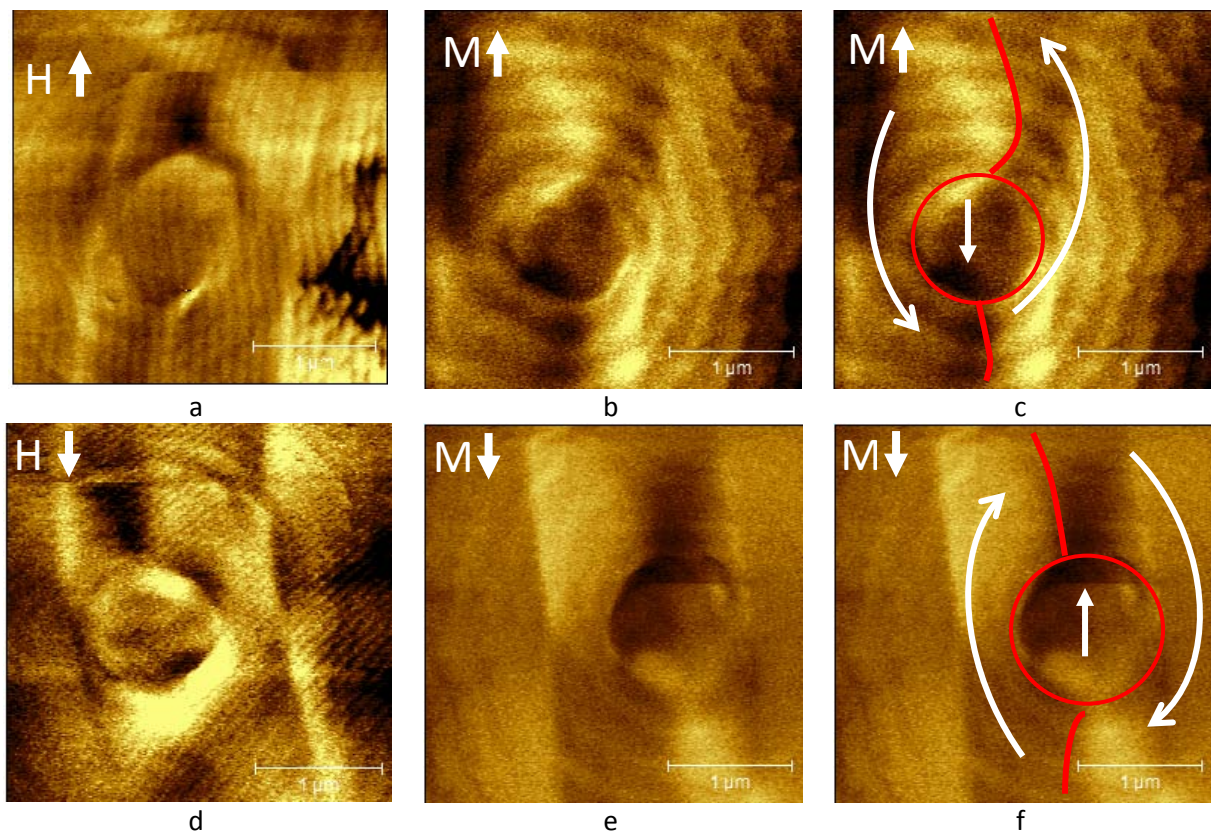


Figure 49: a and d) measurements under a weak field. b and e) Measurements after magnetization with a strong magnetic field. c and f) analyze of the magnetic domains and the stray field.

## 5 CONCLUSION & RECOMMENDATIONS

### 5.1 CONCLUSION

The goal of this project was to be able to control the magnetization at the conical apex of the SF-STM tip and to get an in-plane magnetization at the conical apex. For this the small tip was made to mimic the tip of the SF-STM. Profiles of the tips made by the AFM, shows that the small tip have a corresponding curvature radius as the tips of the SF-STM.

MFM measurements at the small tips showed a similar magnetization as the double tip measurements. The measurements showed an out-of-plane magnetization at the conical apex of the tip. If a magnetic field was applied during the measurements it was possible to force an in-plane magnetization at the conical apex. Either when the applied field was removed, the in-plane magnetization switched back to an out-of-plane magnetization. The cobalt layer had a too weak magnetic remanence for an in-plane magnetization. The conical apex of the tip had in a single domain.

To increase the magnetization two different methods were used viz. evaporation anisotropy and shape anisotropy. The evaporation anisotropy is done by applying a magnetic field during the e-beam evaporation of the magnetic layer. This was done by using a sample holder with two magnets at the edges of the sample. Measurements by the VSM showed a uni-axial anisotropy in the same direction as the applied field during the evaporation. Introduced evaporation anisotropy at the tip showed an increase in remanence.

The second method to increase the remanence of the cobalt film was by introducing shape anisotropy. To shape the magnetic film into a strip, a focused ion beam was used. A FIB depth of 100 nm has been used to ensure that the metal layer stack was fully removed. First the shape anisotropy was analyzed at flat beam structures, which were made by using the FIB. By applying a magnetic field the magnetization was characterized and showed an increase of the remanence by an increasing length/width ratio. The magnetization direction of strips with a small length/width ratio could easily be switched by a applying a magnetic field. Either strips with a large length/width ratio showed a higher coercivity and could only be switched by the strong field of the solid magnet. The weaker field applied by the coil was not sufficient to switch the magnetization direction of the strips with a large length/width ratio.

Shape anisotropy applied to the tips showed a small increase in the magnetic remanence around the conical apex of the tips. Either the in-plane magnetization at the conical apex of the tips under an applied field, switched back to out-of-plane magnetization if the field was removed. Different strips were made with a varying length/width ratio. As seen by the beam high length/width ratios increased the coercivity of the films and introduced an easy-axis in the films in the direction of the strips. Total decoupling of the strip with the rest of the metal layer stack did not show an improvement in the remanence of the in-plane magnetization.

Introducing evaporation anisotropy and shape anisotropy both had an effect at the magnetization of the tip. Both anisotropies have been combined. This tip had a 1  $\mu\text{m}$  wide strip, which was FIB'ed in the direction of the applied field during the evaporation of the cobalt layer. VSM measurements showed that the easy-axis of the film is parallel to this field. The tip was analyzed by MFM and for the

characterization of the magnetization magnetic fields of the coil and the hard magnet were used. With the magnetic field of coil it was possible to magnetize the tip in the direction of the magnetic field, but it was not possible to switch the magnetization direction when the field was turned 180°. The field of the coil was not strong enough. If the tip was magnetized with the stronger field of the hard magnet and then was characterized by the MFM an in-plane magnetization at the conical apex of the tip was visible. If the tip was magnetized 180° by the hard magnet, the magnetization of the cobalt layer turned with the applied field.

The goal to control the magnetization at the conical apex of the pyramid has been realized. By applying evaporation and shape anisotropy it was possible to get an in-plane magnetization at the conical apex of the small tip. During the fabrication of the tip it is possible to control the direction of the magnetic field and strip, which results in the possibility to have a well defined magnetization direction during the measurements in the SF-STM. The shape of the strip should not have an effect on the measurements of the SF-STM, because the conical apex of the tip is the part where the current from substrate to tip tunnels in.

## 5.2 OUTLOOK

The idea of introducing evaporation anisotropy and shape anisotropy in the metal layer stack at the tip worked to realize an in-plane magnetization at the conical apex of the tip. The direction of the in-plane magnetization could be controlled. The idea behind the assignment was to be able to control the magnetization in the tips of the SF-STM, but the principle to control the magnetization in the tips could also be applied in the tips of the SP-STM. The tip will be then a bit blunter as they are now, which has a negative effect for the resolution. Either in a stable system it should be possible to measure the in-plane magnetization of magnetic domains.

Now the magnetization of the cobalt layer at the conical apex can be controlled, the next step is to characterize the electrical characteristic of these tips. The FIB could cause changes in the electronic characteristic of the tips, due to the possibility of charging through the FIB. To characterize the electronic characteristics new tips should be made. This is because the complete silicon oxide is removed before the metal layer stack was evaporated, which result in a large metal-semiconductor interface. For the SF-STM there should only be a metal-semiconductor interface at the conical apex of the tip. Therefore, only the silicon oxide should be removed at the conical apex. If the characteristics are okay, the principal of the strip can be applied at the double tips. These tips can be used in SF-STM measurements at in-plane magnetized samples.

The strip is now made by the use of FIB. This process is a time consuming process, which can be done for a single SF-STM tip a time. Further avoiding the FIB in the process will also prevent negative effects of eventual charging. Therefore producing the strip at the tips by a lithography step will be a solution. For this there could be two different options, namely first deposit the metal layer stack and shape this to a strip, or first shaping the strip in the silicon and then deposit the metal layer stack. The first method is the closest one to this assignment and here the strip is decoupled with the rest of the metal layer stack. This is a similar procedure as it was done in this assignment with the FIB. In this lithography step, after depositing the metals by the DCA, the strip should be defined by a lithography step. Then an Ion beam etch step can be used to remove the metals next to the strip and so decouple the strip at the sides.

In the second method there is no decoupling between the strip and the rest of the cobalt layer at the tip. That this could be possibility is based on the single domain at the conical apex of the tips. It could be a possibility that the step at the side of the strip introduce the shape anisotropy in the cobalt layer. This sequence will results in first defining the shape in the photo resist by the lithography step. Then the silicon can be etched by RIE. After making the strip the deposition of the metals can be done.

The height of the tips and the resolution in the x-y plane will be two challenges which should be solved in the lithography step. For the first challenge there are different solutions, like using the negative photoresist SU-8 which can be spun thick enough to cover the small tips and also in a later stage the double tips. Another method is to use a resist coater, which can cover the tips with a thin layer of resist. In both methods the tips could completely be covered by photoresist. Then the mask could be made with the right pattern to define the strip at the pyramids. The other problem is that in the x-y plane a resolution is needed of about 1  $\mu\text{m}$ , which is about the limit of the mask aligner. So it will need some practice and clear align marks to control the place of the strip. This should need some practice.

## 6 LITERATURE

- [1] Multiterminal semiconductor/ferromagnet probes for spin-filter scanning tunneling microscopy; I. J. Vera Marún et al.; journal of applied physics; 105, 2009
- [2] Scanning Probe Microscopy and Spectroscopy; R. Wiesendanger; Cambridge University Press; 1994; ISBN: 0 52141810 0
- [3] Scanning tunneling microscopy; Institut für Experimentelle und Angewandte Physik der Universität Kiel
- [4] Spintronics: Fundamentals and applications; I. Zutic et al.; Rev. of Modern Physics; 76; 2004; 323-410
- [5] Observation of vacuum tunneling of spin-polarized electrons with the scanning tunneling microscope; R. Wiesendanger et al.; Physical reviews letters; 65; 1990; 247-250
- [6] Real-Space Imaging of Two-Dimensional Antiferromagnetism on the Atomic Scale; S. Heinze et al.; Science; 288; 2000; 1805-1808
- [7] Ballistic electron microscopy and spectroscopy of metal and semiconductor nanostructures; W. Yi et al.; Surface Science Reports; 64; 2009; 169-190
- [8] Ballistic electron magnetic microscopy: Imaging magnetic domains with nanometer resolution; W.H. Rippard et al.; applied physics letters; 75; 1999; 1001-1003
- [9] SPIN-FILTER SCANNING TUNNELING MICROSCOPY; Iván Jesús Vera Marún; Wöhrmann Print Service; 2010; ISBN: 978-90-365-3024-8
- [10] Magnetic Domains; Chapter 3; A. Hubert; Springer Berlin Heidelberg New York; 1998; ISBN: 978-3-540-64108-7
- [11] Magnetic Domains; Chapter 2; A. Hubert; Springer Berlin Heidelberg New York; 1998; ISBN: 978-3-540-64108-7
- [12] Atomic force microscopy (AFM); Department of Pharmacy; Uppsala University
- [13] Functionality and dynamics of deposited metal nanoclusters, S.A. Koch; Groningen University Press; 2005; ISBN 90-367-2289-6
- [14] On the determination of the internal magnetic structure by magnetic force microscopy; B. Vellekoop et al.; Journal of Magnetism and Magnetic Materials; 190; 1998; 148-151
- [15] Getting the most from your vibrating sample magnetometer; Dennis Speliotis; ADE Technologies
- [16] Spin-Dependent Hot Electron Transport in Co\_Cu Thin Films; W.H. Rippard et al; Physical review letters; 84; 2000; 971-974
- [17] Magnetoelectronics; G. Prinz; Science; 282; 1998; 1660-1663

## ACKNOWLEDGEMENTS

In this part I would like to thank all the people who helped me during my master assignment.

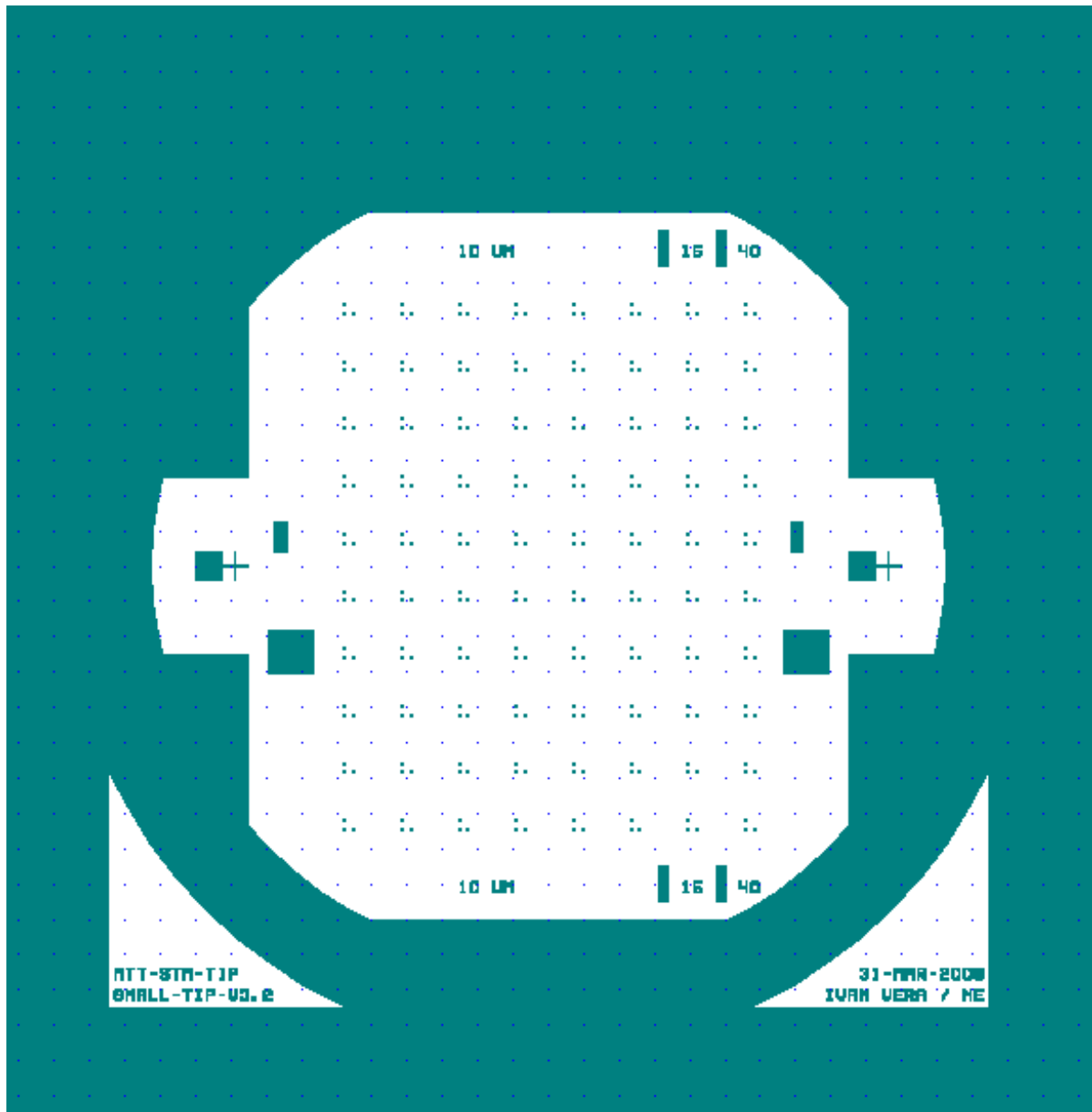
First I would like to thank the members of my Graduation committee. Thanks to Wilfred van der Wiel and Iván Vera Marún for the supervision of my assignment. Also I would like to thank Johnny Sanderink and Martin Siekman for the technical help and the advice during my assignment. Also thanks to Paul Kelly for being the external member in the committee.

Further I would like to thank the NanoElectronics Group for the nice time during my Master assignment. The group gave a great opportunity for me to get my first experience in the clean room and to work at an interesting assignment. Further I would also thank the cleanroom staff and Henk van Wolferen and Kees Ma for their help during my assignment.

Next I would like to thank my fellow student from the master Nanotechnology for the nice two years during my master. Especially I would like to mention my fellow members of the INASCON 2010 committee, who helped to make it possible to organize it. At last I would like to thank all the Master students from NE and TST over the last year for the good times in the student room and at the coffee machine.

## APPENDIX A: MASK

MASK: MTT-STM-TIP\_SMALL-TIP-V3.2



APPENDIX B: CLEANROOM PROCESS

Step	Process	Comment
1	<p><b>Substrate selection - Silicon &lt;100&gt; DSP</b> (#subs002)</p> <p>CR112B / Wafer Storage Cupboard Supplier: Orientation: &lt;100&gt; Diameter: 100mm Thickness: 525<math>\mu</math>m +/- 25<math>\mu</math>m Polished: Double side Resistivity: 5-10<math>\Omega</math>cm Type: p</p>	
2	<p><b>Cleaning Standard</b> (#clean003)</p> <p>CR112B / Wet-Bench 131 HNO<sub>3</sub> (100%) Selectipur: MERCK HNO<sub>3</sub> (69%) VLSI: MERCK</p> <ul style="list-style-type: none"> <li>• Beaker 1: fuming HNO<sub>3</sub> (100%), 5min</li> <li>• Beaker 2: fuming HNO<sub>3</sub> (100%), 5min</li> <li>• Quick Dump Rinse &lt;0.1<math>\mu</math>S</li> <li>• Beaker 3: boiling (95°C) HNO<sub>3</sub> (69%), 10min</li> <li>• Quick Dump Rinse &lt;0.1<math>\mu</math>S</li> <li>• Spin drying</li> </ul>	
3	<p><b>Etching HF (1%) Native Oxide</b> (#etch027)</p> <p>CR112B / Wet-Bench 3-3 HF (1%) VLSI: MERCK 112629.500</p> <ul style="list-style-type: none"> <li>• Etch time: &gt;1min</li> <li>• Quick Dump Rinse &lt;0.1<math>\mu</math>S</li> <li>• Spin drying</li> </ul>	
4	<p><b>Dry Oxidation at 1100°C of Silicon</b> (#depo037)</p> <p>CR112B / Furnace A2 Only for dedicated processing (CMOS) Standby temperature: 700°C</p> <ul style="list-style-type: none"> <li>• Program: DRY1100C</li> <li>• See Calibration curve on MIS page</li> <li>• Temp.: 1100°C</li> <li>• Gas: O<sub>2</sub></li> <li>• Flow: ?l/min</li> </ul>	
5	<p><b>LPCVD Si<sub>3</sub>N<sub>4</sub> stoichiometric</b> (#depo001)</p> <p>CR125C / Tempress LPCVD F1</p> <p>A flush purge of 2.5 hr is needed before deposition Tube: F1</p> <ul style="list-style-type: none"> <li>• Program: Nitr01</li> <li>• SiH<sub>2</sub>Cl<sub>2</sub> flow: 22sccm</li> <li>• NH<sub>3</sub> flow: 66sccm</li> <li>• temperature: 800°C</li> <li>• pressure: 200mTorr</li> <li>• Stress: 1,09 ± 40 MPa</li> <li>• deposition rate: 4-6 nm/min</li> <li>• N<sub>f</sub>: 2.008</li> </ul>	
6		Annealing in N2
7	<p><b>Lithography – Priming liquid</b></p> <p>Cr112B / Delta 20 Hotplate 120 HexaMethulDislazane (HDMS) Dehydration bake 120 degrees 5minutes Spin program 4</p>	1 minute prebake at 120 degrees

8	<b>Lithography - Coating Olin907-17</b> (#lith005)	CR112B / Suss Micro Tech Spinner (Delta 20) Hotplate 95 °C Olin 907-17 • Spin Program: 4 (4000rpm, 20sec) • Prebake (95°C): 90s
9	<b>Lithography - Alignment &amp; Exposure Olin 907-17 (EV620)</b> (#lith021)	CR117B / EV620 Electronic Vision Group 620 Mask Aligner • Hg-lamp: 12 mW/cm <sup>2</sup> • Exposure Time: 4sec
10	<b>Lithography - Dehydration bake SU-8</b> (#lith062)	CR112B / Hotplate • Dehydration bake (120°C): 10min
11	<b>Plasma etching SiN (Etske)</b> (#etch004)	CR102A / Elektrotech PF310/340 Dirty chamber Styros electrode • Electrode temp.: 10°C • CHF <sub>3</sub> flow: 25sccm • O <sub>2</sub> flow: 5sccm • pressure: 10mTorr • power: 75W Etchrate SiN = 50nm/min (for V <sub>DC</sub> =-460V) Etchrate SiN = 75 nm/min (for V <sub>DC</sub> = -580V) Etchrate Olin resist = 95nm/min If DC-Bias < 375V apply chamber clean (#etch003)
12	<b>Cleaning Standard</b> (#clean003)	CR112B / Wet-Bench 131 HNO <sub>3</sub> (100%) Selectipur: MERCK HNO <sub>3</sub> (69%) VLSI: MERCK • Beaker 1: fuming HNO <sub>3</sub> (100%), 5min • Beaker 2: fuming HNO <sub>3</sub> (100%), 5min • Quick Dump Rinse <0.1μS • Beaker 3: boiling (95°C) HNO <sub>3</sub> (69%), 10min • Quick Dump Rinse <0.1μS • Spin drying
13	<b>Etching BHF (1:7) SiO<sub>2</sub></b> (#etch024)	CR112B / Wet-Bench 3-3 NH <sub>4</sub> F/HF (1:7) VLSI: BASF • Quick Dump Rinse <0.1μS • Spin drying Etchrate thermal SiO <sub>2</sub> = 60-80nm/min Etchrate PECVD SiO <sub>2</sub> = 125/nm/min Etchrate TEOS SiO <sub>2</sub> = 180/nm/min
14	<b>Etching of Silicon by KOH - standard</b> (#etch038)	CR102B / KOH KOH: MERCK 105019.500 KOH:DI = (1:3) 25wt% KOH: 500g KOH pellets in 1500ml DI water • Temp.: 75°C • Stirrer • Quick Dump Rinse <0.1μS • Spin drying Etchrates: Si <100> = 1μm/min Si <111> = 12.5nm/min

## Controlling the magnetization at the conical apex of a multi-terminal STM probe

		SiO <sub>2</sub> (thermal) = 180nm/hr SiRN < 0.6nm/hr	
15	<b>Cleaning RCA-2 (HCL/H<sub>2</sub>O<sub>2</sub>/H<sub>2</sub>O)</b> (#clean007)	CR112B / Wet-Bench 130 HCL (36%) Selectipur, BASF H <sub>2</sub> O <sub>2</sub> (31%) VLSI, BASF Only use the dedicated wafer carriers and rod! HCL:H <sub>2</sub> O <sub>2</sub> :H <sub>2</sub> O (1:1:5) vol% <ul style="list-style-type: none"> <li>• add HCL to H<sub>2</sub>O</li> <li>• add H<sub>2</sub>O<sub>2</sub> when mixture at 70°C</li> <li>• temperature 70-80°C</li> <li>• cleaning time 10-15min</li> <li>• Quick Dump Rinse &lt;0.1μS</li> <li>• Spin drying</li> </ul>	RCA2 cleaning
16	<b>Cleaning Standard</b> (#clean003)	CR112B / Wet-Bench 131 HNO <sub>3</sub> (100%) Selectipur: MERCK HNO <sub>3</sub> (69%) VLSI: MERCK <ul style="list-style-type: none"> <li>• Beaker 1: fuming HNO<sub>3</sub> (100%), 5min</li> <li>• Beaker 2: fuming HNO<sub>3</sub> (100%), 5min</li> <li>• Quick Dump Rinse &lt;0.1μS</li> <li>• Beaker 3: boiling (95°C) HNO<sub>3</sub> (69%), 10min</li> <li>• Quick Dump Rinse &lt;0.1μS</li> <li>• Spin drying</li> </ul>	
17	<b>Etching HF (1%) Native Oxide</b> (#etch027)	CR112B / Wet-Bench 3-3 HF (1%) VLSI: MERCK 112629.500 <ul style="list-style-type: none"> <li>• Etch time: &gt;1min</li> <li>• Quick Dump Rinse &lt;0.1μS</li> <li>• Spin drying</li> </ul>	
18	<b>Dry Oxidation at 1100°C of Silicon</b> (#depo037)	CR112B / Furnace A2 Only for dedicated processing (CMOS) Standby temperature: 700°C <ul style="list-style-type: none"> <li>• Program: DRY1100C</li> <li>• See Calibration curve on MIS page</li> <li>• Temp.: 1100°C</li> <li>• Gas: O<sub>2</sub></li> <li>• Flow: ?l/min</li> </ul>	
19	<b>Cleaning Standard</b> (#clean003)	CR112B / Wet-Bench 131 HNO <sub>3</sub> (100%) Selectipur: MERCK HNO <sub>3</sub> (69%) VLSI: MERCK <ul style="list-style-type: none"> <li>• Beaker 1: fuming HNO<sub>3</sub> (100%), 5min</li> <li>• Beaker 2: fuming HNO<sub>3</sub> (100%), 5min</li> <li>• Quick Dump Rinse &lt;0.1μS</li> <li>• Beaker 3: boiling (95°C) HNO<sub>3</sub> (69%), 10min</li> <li>• Quick Dump Rinse &lt;0.1μS</li> <li>• Spin drying</li> </ul>	
20	<b>Etching BHF (1:7) SiO<sub>2</sub></b> (#etch024)	CR112B / Wet-Bench 3-3 NH <sub>4</sub> F/HF (1:7) VLSI: BASF <ul style="list-style-type: none"> <li>• Quick Dump Rinse &lt;0.1μS</li> <li>• Spin drying</li> </ul> Etchrate thermal SiO <sub>2</sub> = 60-80nm/min Etchrate PECVD SiO <sub>2</sub> = 125/nm/min Etchrate TEOS SiO <sub>2</sub> = 180/nm/min	To remove native silicon nitride oxide

21	<p><b>Etching of SiN (Hot H<sub>3</sub>PO<sub>4</sub>)</b> (#etch053)</p>	<p>CR112B / Wet-Bench 3-1 H<sub>3</sub>PO<sub>4</sub> 85% Merck VLSI 1.00568.2500 Apply always first a Standard Wafer Clean (#clean003) and a 1% HF dip (#etch027) to remove native oxide.</p> <ul style="list-style-type: none"> <li>• Temp.: 180°C (caution!)</li> <li>• Quick Dump Rinse &lt;0.1μS</li> <li>• Spin drying</li> </ul> <p>Etchrate SiRN: 3.5 nm/min High selective for SiO<sub>2</sub> layers Only SiO<sub>2</sub>, Silicon, PolySilicon, SiRN, SiON, SiON are allowed.</p> <table border="1" data-bbox="560 584 1082 797"> <thead> <tr> <th>Temperature [°C]</th> <th>etch rate Si<sub>x</sub>N<sub>y</sub> [nm/min]</th> <th>etch rate (SiO<sub>2</sub>) [nm/min]</th> </tr> </thead> <tbody> <tr> <td>180</td> <td>4.1</td> <td>0.48</td> </tr> <tr> <td>160</td> <td>1.4</td> <td>0.16</td> </tr> <tr> <td>140</td> <td>0.5</td> <td>0.05</td> </tr> </tbody> </table>	Temperature [°C]	etch rate Si <sub>x</sub> N <sub>y</sub> [nm/min]	etch rate (SiO <sub>2</sub> ) [nm/min]	180	4.1	0.48	160	1.4	0.16	140	0.5	0.05	
Temperature [°C]	etch rate Si <sub>x</sub> N <sub>y</sub> [nm/min]	etch rate (SiO <sub>2</sub> ) [nm/min]													
180	4.1	0.48													
160	1.4	0.16													
140	0.5	0.05													
22	<p><b>Etching HF (1%) Native Oxide</b> (#etch027)</p>	<p>CR112B / Wet-Bench 3-3 HF (1%) VLSI: MERCK 112629.500</p> <ul style="list-style-type: none"> <li>• Etch time: &gt;1min</li> <li>• Quick Dump Rinse &lt;0.1μS</li> <li>• Spin drying</li> </ul>	for pad oxide removal												
23	<p><b>Cleaning Standard</b> (#clean003)</p>	<p>CR112B / Wet-Bench 131 HNO<sub>3</sub> (100%) Selectipur: MERCK HNO<sub>3</sub> (69%) VLSI: MERCK</p> <ul style="list-style-type: none"> <li>• Beaker 1: fuming HNO<sub>3</sub> (100%), 5min</li> <li>• Beaker 2: fuming HNO<sub>3</sub> (100%), 5min</li> <li>• Quick Dump Rinse &lt;0.1μS</li> <li>• Beaker 3: boiling (95°C) HNO<sub>3</sub> (69%), 10min</li> <li>• Quick Dump Rinse &lt;0.1μS</li> <li>• Spin drying</li> </ul>													
24	<p><b>Etching BHF (1:7) SiO<sub>2</sub></b> (#etch024)</p>	<p>CR112B / Wet-Bench 3-3 NH<sub>4</sub>F/HF (1:7) VLSI: BASF</p> <ul style="list-style-type: none"> <li>• Quick Dump Rinse &lt;0.1μS</li> <li>• Spin drying</li> </ul> <p>Etchrate thermal SiO<sub>2</sub> = 60-80nm/min Etchrate PECVD SiO<sub>2</sub> = 125/nm/min Etchrate TEOS SiO<sub>2</sub> = 180/nm/min</p>	For removal top of the oxide layer												
25	<p><b>Cleaning Standard</b> (#clean003)</p>	<p>CR112B / Wet-Bench 131 HNO<sub>3</sub> (100%) Selectipur: MERCK HNO<sub>3</sub> (69%) VLSI: MERCK</p> <ul style="list-style-type: none"> <li>• Beaker 1: fuming HNO<sub>3</sub> (100%), 5min</li> <li>• Beaker 2: fuming HNO<sub>3</sub> (100%), 5min</li> <li>• Quick Dump Rinse &lt;0.1μS</li> <li>• Beaker 3: boiling (95°C) HNO<sub>3</sub> (69%), 10min</li> <li>• Quick Dump Rinse &lt;0.1μS</li> <li>• Spin drying</li> </ul>													
26	<p><b>Etching HF (1%) Native Oxide</b> (#etch027)</p>	<p>CR112B / Wet-Bench 3-3 HF (1%) VLSI: MERCK 112629.500</p> <ul style="list-style-type: none"> <li>• Etch time: &gt;1min</li> <li>• Quick Dump Rinse &lt;0.1μS</li> <li>• Spin drying</li> </ul>	With fresh solution												

27	<b>Recipe description</b> Sputtering of Co (#depo047)	Eq.Nr. 37 / Sputterke Co Target (gun #: see mis logbook) <ul style="list-style-type: none"><li>• Electrode temp.: water cooled electrode</li><li>• Ar flow: app. 80 sccm, pressure depending!</li><li>• Base pressure: &lt; 1.0 e-6mbar</li><li>• Sputter pressure: 6.6 e-3mbar</li><li>• power: 50W</li><li>• Depositionrate = 3.3 nm/min</li></ul>	
----	---	---	--